HIGH ENERGY NEUTRAL ATOM (HENA) IMAGER

FOR THE

IMAGE MISSION

D. G. MITCHELL, S. E. JASKULEK, C. E. SCHLEMM, E. P. KEATH, R. E. THOMPSON, B. E. TOSSMAN, J. D. BOLDT, J. R. HAYES, G. B. ANDREWS, AND N. PASCHALIDIS

The Johns Hopkins University Applied Physics Laboratory

D. C. HAMILTON, R. A. LUNDGREN, E. O. TUMS, P. WILSON IV,

The University of Maryland

H. D. VOSS, D. PRENTICE

Taylor University

K. C. HSIEH, C. C. CURTIS

The University of Arizona

F. R. POWELL

Luxel Corporation

TABLE OF CONTENTS

Abstract: The IMAGE mission will be the first of its kind, designed to comprehensively image a variety of emissions from the Earth's magnetosphere, with sufficient time resolution to follow the dynamics associated with the development of magnetospheric storms. Energetic neutral atoms (ENA) emitted from the ring current during storms are one of the key emissions that will be imaged. This paper describes the characteristics of the High Energy Neutral Atom imager, HENA.

Using pixelated solid state detectors, imaging microchannel plates, electron optics, and time of flight electronics, HENA is designed to return images of the ENA emitting regions of the inner magnetosphere with 2 minute time resolution, at angular resolution of 8 degrees or better above the energy of ~ 50 keV/nucleon. HENA will also image separately the emissions in hydrogen, helium, and oxygen above 30 keV/nucleon. HENA will reject energetic ions below 200 keV/charge, allowing ENA images to be returned in the presence of ambient energetic ions.

HENA images will reveal the distribution and the evolution of energetic ion distributions as they are injected into the ring current during geomagnetic storms, as the drift about the Earth on both open and closed drift paths, and as they decay through charge exchange to pre-storm levels. Substorm ion injections will also be imaged, as will the regions of low altitude, high latitude ion precipitation into the upper atmosphere.

1. Introduction

Charge exchange interactions between energetic trapped ions and cold ambient neutral exospheric gasses result in the creation of Energetic Neutral Atoms (ENAs) in the Earth's magnetosphere. These ENAs then escape the magnetospheric system since they are no longer trapped, and a detector using straight-path optics may be used to form global images of the emission regions, and thus of the magnetospheric system. Various reviews of this subject have been published, including those by McEntire and Mitchell, 1989, Keath *et al.*, 1989, Williams *et al*., 1992, McComas *et al*., 1992, McComas *et al*., 1994, Funsten *et al.*, 1994, Gruntman, 1997, McComas *et al*., 1998, and Hsieh and Curtis, 1998.

The science requirements driving the Neutral Atom Imaging (NAI) instrumentation for IMAGE are (1) to image the inner magnetosphere including the ring current on a time scale of 300 seconds and (2) to resolve the major species contributing to neutral atom fluxes. To meet these requirements the suite of three NAI instruments provides angle, energy, and composition-resolved images at energies from 10 eV to 500 keV.

IMAGE carries three NAI instruments because of the different techniques that apply to low (0.01 to 0.5 keV), medium (1 to 30 keV), and high (30 to 500 keV) energy neutral atoms. This paper describes the instrument that covers the highest of these energy ranges, the High Energy Neutral Atom imager, HENA. Charge exchange neutrals in this energy range have been detected by energetic ion detectors on several Earth orbiting spacecraft: on IMP 8 and ISEE-1 (Roelof *et al.*, 1985, Roelof 1987); on the Swedish microsatellite Astrid (Barabash *et al*., 1998, C:son Brandt *et al*., 1999a, b), on the ISTP Geotail spacecraft, using the EPIC instrument (Lui *et al.*, 1996), and most recently in the images returned by the CEPPAD detector on the ISTP Polar spacecraft (Henderson *et al.*, 1997). ENA fluxes during storm time are therefore relatively well known, and contributed to the HENA design parameters.

The HENA instrument owns considerable heritage to the Cassini Magnetosphere Imaging Instrument Ion and Neutral Camera (INCA) (Krimigis *et al*., 1999; Mitchell *et al*., 1993; 1998).

a)

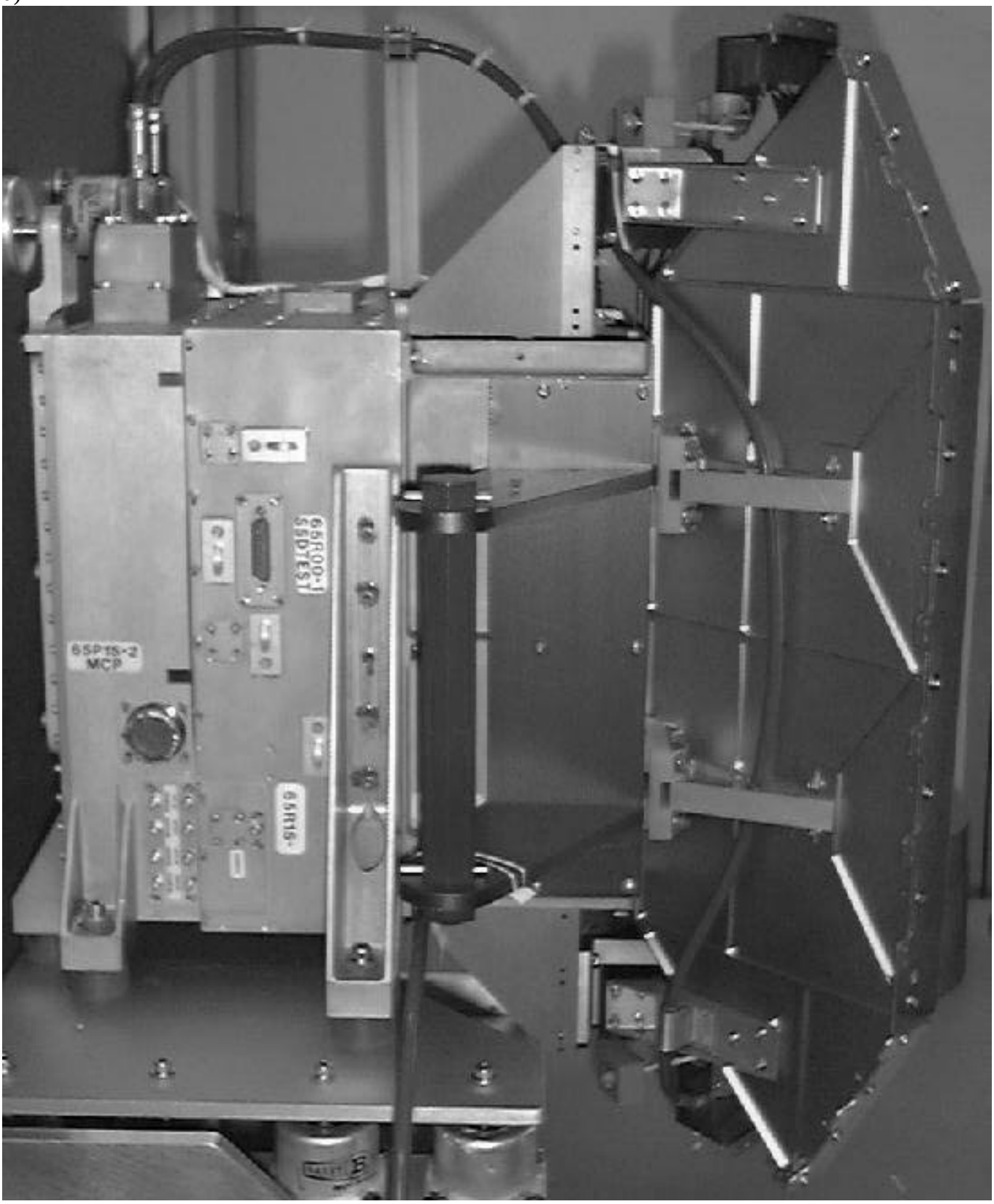

b)

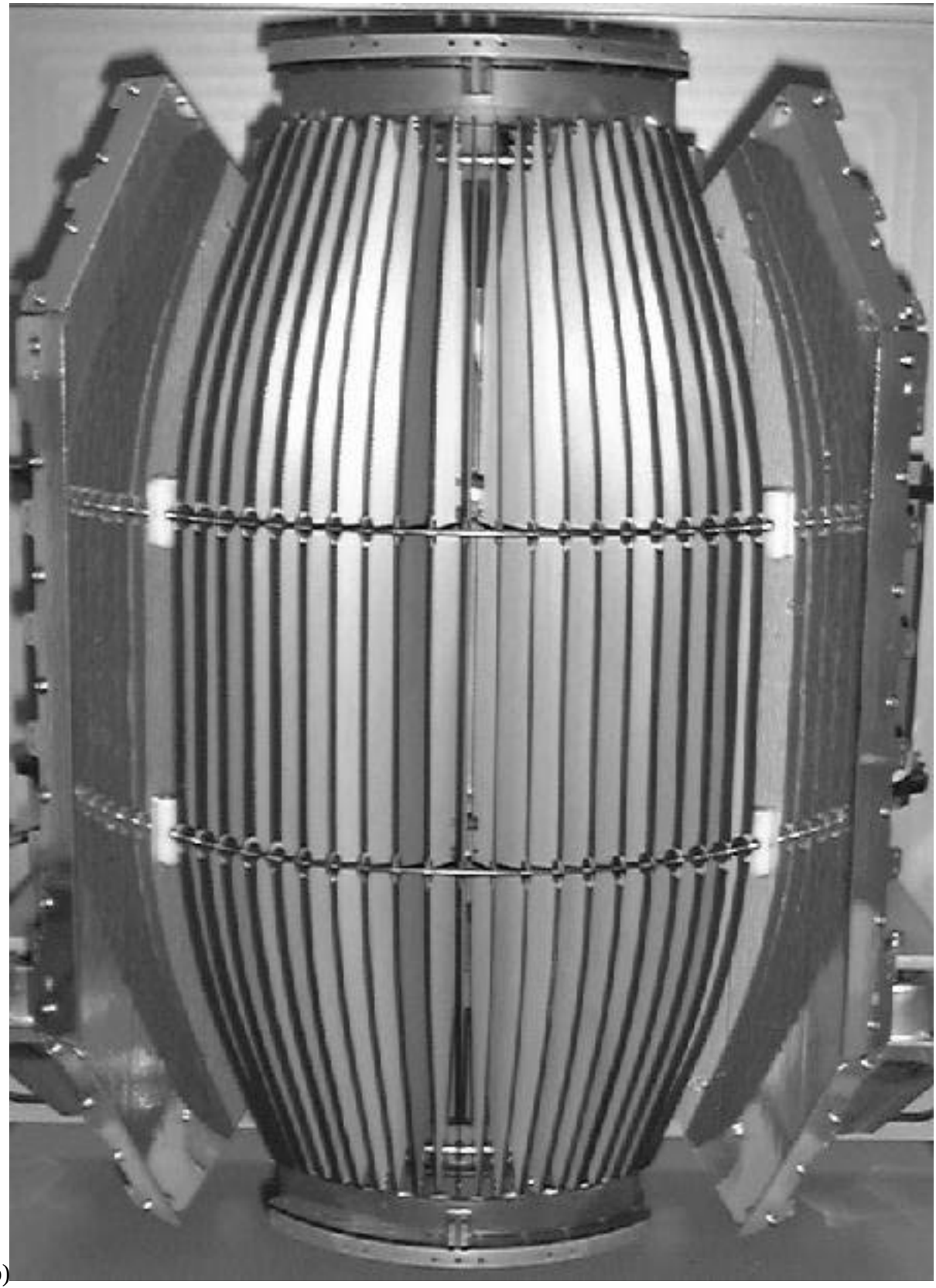

Figure1. (a) HENA instrument at delivery to SWRI for integration on the deckplate; *(b)* HENA view into aperture. The spacecraft spin vector is vertical in both (a) and (b).

HENA (Figure 1) is a slit camera with a 90˚ x 120˚ field of view and a segmented back plane incorporating an imaging solid-state detector (SSD) array in one portion and a microchannel plate (MCP) with position-sensitive anode in the other. Pulse height analysis of the SSD pulses provides total energy, which, combined with the measured time of flight (TOF) velocity determination, yields neutral atom mass. As a redundancy feature, the MCP pulses may also be pulse-height analyzed, yielding sufficient separation of species to separate H and O, although this capability would only be implemented in software should the SSD system suffer a failure. Each pixel in the plane of the sky is viewed both by the SSD array and the MCP as the scene is scanned during each spacecraft spin (spin period 2 minutes, spin axis to the orbit plane). HENA acquires angular images by spatially locating the start pulses on the entrance slit and the stop pulses in the rear sensor plane, which constrains the ENA trajectory. Based on its trajectory, velocity, and species, the appropriate pixel in the stored sky-map image is incremented. The collimator serves to suppress charged particle entry by biasing adjacent collimating plates at ± 4 kV.

The Earth environment UV background is suppressed by a combination of (1) a Si-polyimide-C foil that reduces the UV flux, (2) the relative insensitivity of the SSD to UV photons, and (3) the triple coincidence timing requirement between the start MCP, coincidence MCP, and the back plane detector (either the MCP or the SSD). Solar UV is mitigated through use of a moveable shutter and if necessary by modulation of MCP voltage (discussed in Section 2.1.7). See Funsten *et al.*, 1998 for a complete discussion of UV rejection techniques appropriate for ENA imaging.

All HENA potentials are static except for infrequent adjustments of MCP gain. After activation and checkout, HENA runs in a single operational mode. Some choices of data product priorities can be made as software options, providing, for example, a periodic (e.g., monthly) calibration mode to check the TOF/PH identification of atomic species, the pulse-amplifier chains, and the binning logic.

1.1 SCIENCE REQUIREMENTS

The HENA Instrument is designed to collect images of energetic, magnetospheric ion populations by identifying energetic neutral atoms according to their direction of arrival, mass, and velocity. The characteristics of HENA, i.e. its resolutions in energy, mass and direction, field of view, and sensitivity, will allow the collection of images as described in Sections 2 and 3.

The processes responsible for Earth's aurora are to be investigated, substorm processes will be imaged with sufficient time resolution to follow dynamics, and the origins of the magnetospheric hot plasmas will be investigated. HENA essentially treats the escaping charge exchange neutrals like photons to form images of the emitting regions.

A model of the ENA emission in the HENA energy range is shown in Fig. 2, to illustrate some of the features expected in HENA images. This model is shown at high resolution (1 degree pixel size) so that the relevant features are clear. Although HENA provides much coarser angular resolution, the white circles calling out various features represent the pixel size required to detect each of those features. The major structures of the storm-time ring current can be resolved by an imager with ~1R_E resolution. From apogee, 1 R_E corresponds to ~9° resolution. HENA exceeds this resolution throughout most of its energy range. The auroral zone structures can only be resolved from near perigee.

As for sensitivity, Figure 3 shows the simulated HENA counts for an image taken during a large geomagnetic storm, based on measurements taken by the medium energy particle instrument (MEPI, Williams *et al.*, 1978) on the International Sun-Earth Explorer spacecraft on September 29, 1978. The peak pixels in the image (those in the darker area at the center of the bright emission) are over 10,000 counts per pixel, while the lowest counts discernible in this image are still ~50 counts/pixel. Thus, HENA will have adequate sensitivity to follow magnetospheric dynamics at the highest time resolution afforded by the spacecraft spin period of 2 minutes. Of course, there is no structure present in the HENA simulation other than what was resolved by the original MEPI measurements, at ~20 degree resolution.

Furthermore, calculations by Hesse and Birn (1998) indicate that the HENA instrument should be useful in following substorm injection from the near-Earth magnetotail region.

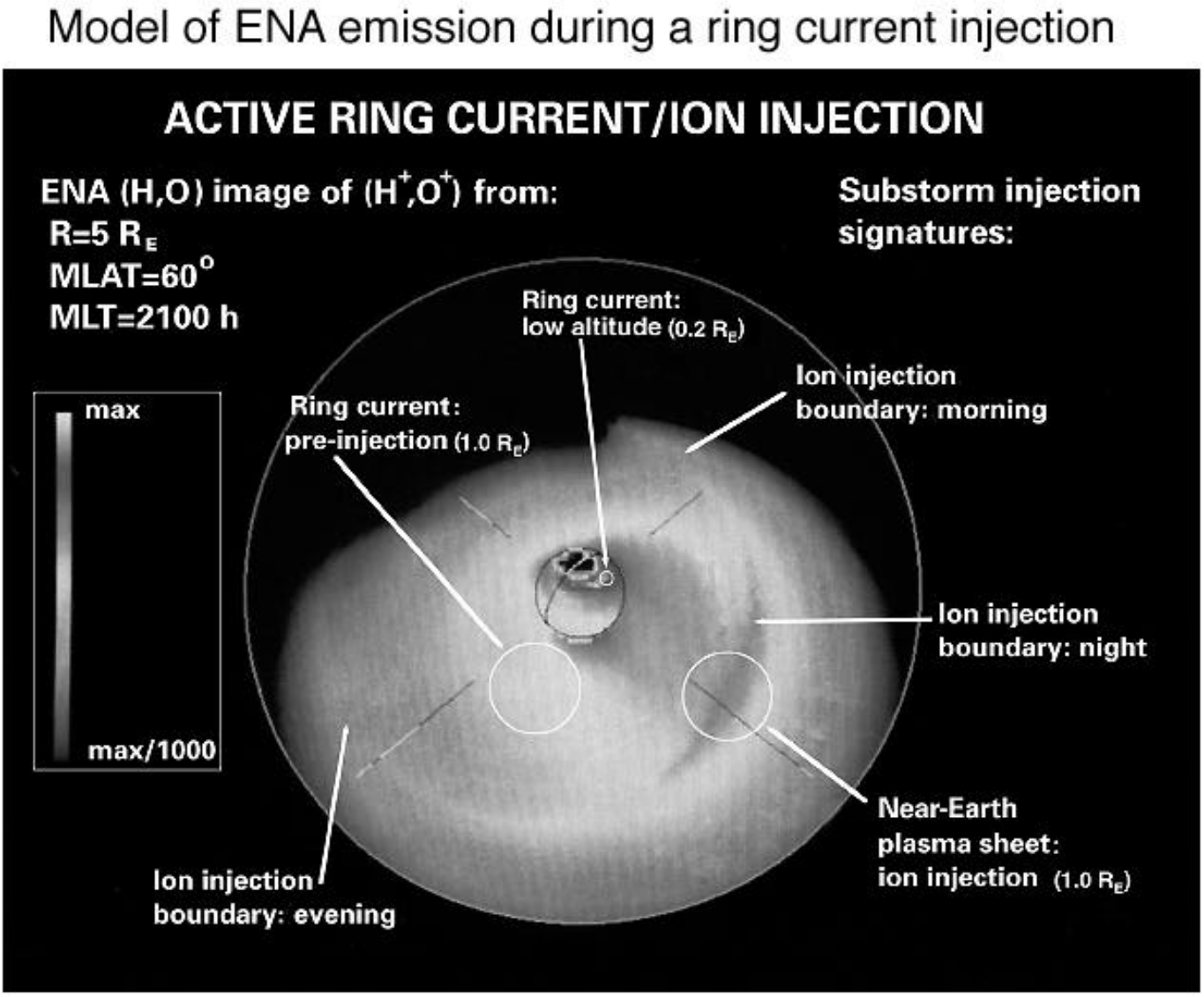

Figure 2 Model ENA emission from the Earth's magnetosphere, in the HENA energy range. Features of interest are labeled. (Figure courtesy of E. C. Roelof)

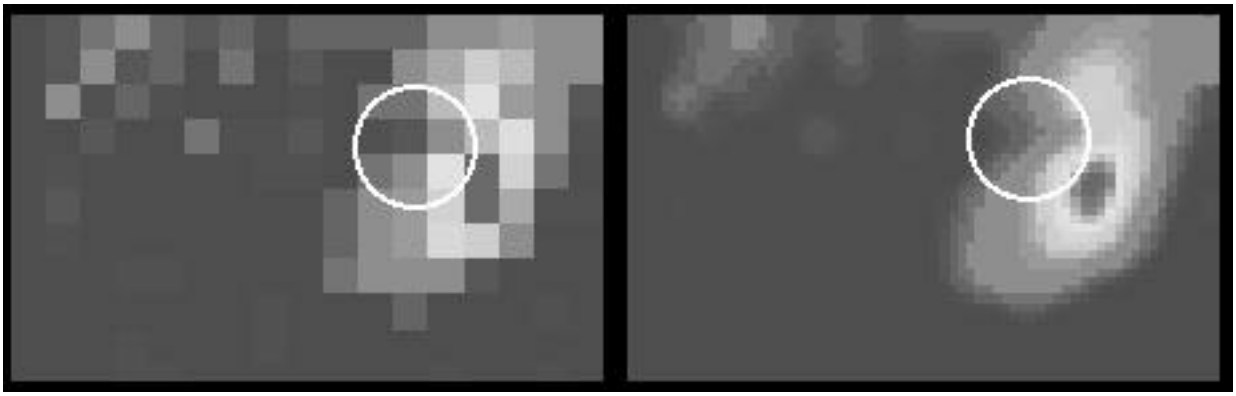

Figure 3. Original ISEE/MEPI data taken September 29, 1978 from 1.7 R_E altitude on left, simulated two minute HENA image of the same geomagnetic storm at HENA angular resolution on the right. The peak counts/pixel expected from HENA for such a storm would be well over 10,000. The Earth's limb is represented by the white circle.

The HENA is designed to meet or contribute to the following IMAGE Mission scientific objectives:

IMAGE Mission Objective	Data Products	Science Product
Global Morphology of Earth's Magnetosphere	ENA Images	(a) direct inference, (b) quantitative forward modeling of images, and (c) image inversion.
Plasma Source Identification	Composition Spectra	(a) ENA source region species identification, (b) source process modeling.
Plasma Energization	ENA Images And Energy Analysis	(a) location and evolution of plasma injections, (b) spatial and temporal evolution of spectra.
Substorms and Plasma Convection	HENA Images	(a) time series determination of motions, density changes and stresses within ~10 R_E of Earth, (b) global views of plasma flows and convection electric fields.
Trapped Radiation Dynamics	HENA Images	(a) diffusive transport, and (b) drift shell features.
Auroral Energy Source	HENA Images	(a) ion precipitation locations and intensities, (b) global energy deposition.

Heliospheric Shocks & Corotating Interaction Regions	HENA Images	charge-exchange between shock-heated plasma and cold interstellar neutrals may provide information on the 3-D structure of heliospheric shocks and co-rotating interaction regions.

2. HENA Imager

2.1 HENA SENSOR

HENA is a sensitive [geometric factor (G) ~1.6 cm^2-sr, and efficiency (ε) from ~0.2 for hydrogen to ~0.9 for oxygen] imaging sensor that analyzes separately the composition, speed, and direction of motion of incident energetic neutral atoms. Elements of the detector assembly can be seen in Figure 4. Greater detail on mechanical envelope and dimensions can be found in Appendix A.

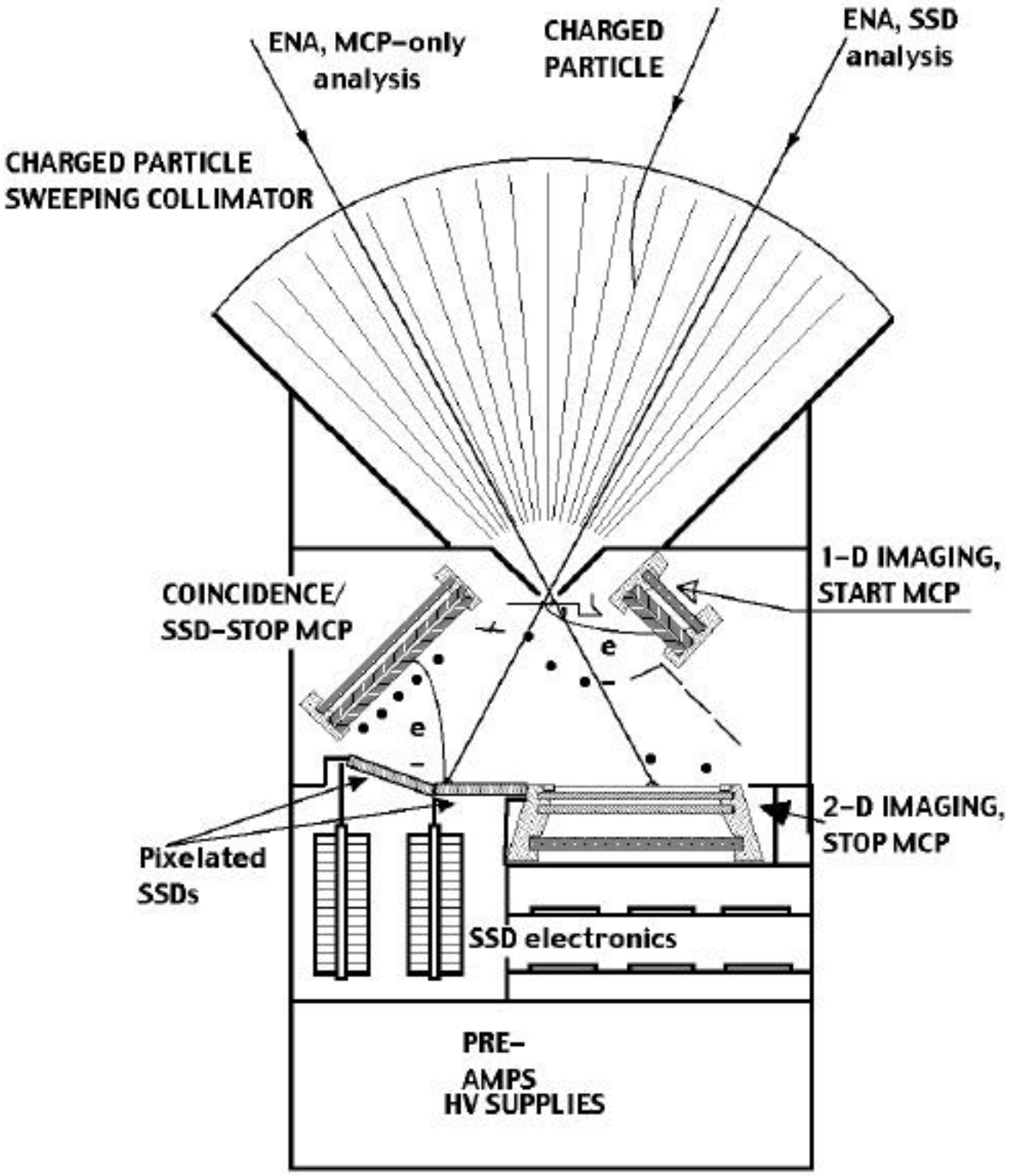

Figure 4. Schematic of the HENA head. Electrically-biased and serrated collimator plates provide the electric field to sweep charged particles out of the entrance slit. Those ENAs penetrating the front foil that covers the entrance slit, produce secondary electrons from the foil to trigger the 1-D imaging and start

MCP. The same ENAs travel to either the SSD or the back foil and the 2-D imaging MCP immediately behind it. Secondary electrons produced by the arriving ENAs at either the SSD or the front of the back foil are steered to trigger the coincidence/SSD-stop MCP. The dots indicate the locations of the wire electrodes for steering the secondary electrons to their respective MCPs. The spacecraft spin vector is perpendicular to plane of the figure.

The HENA sensor characteristics are summarized in Table 2.1-1. The straight rays through the entrance slit to the back plane define a FOV of 90° in azimuth (φ, defined in the spin plane), and 120° in elevation (θ, which varies in the planes containing the collimator plates, perpendicular to φ, centered on the spin plane). The deflection plates do not collimate the FOV; they simply reduce sensitivity in the φ directions they partially obscure.

Table 2.1-1: Energetic neutral atoms or ions, chosen by command

Energy range	~20 keV - 500 keV/nuc.
Energy resolution [$\Delta E/E$]	≤ 0.25
Velocity resolution	~50 km/sec (1ns TOF)
Composition	H, He, O, Heavies
Field Of View	120° x 90°
Angular coverage	~3π sr, spinning
Angular resolution ($\Delta\varphi\Delta\theta$)	~4° x 6°, high energy (>80 keV/nuc)
Angular resolution is degraded by ENA scattering in foils at low E	<8° x <12° above ~40 keV/nuc (see Figure 8)
Time resolution (statistics limited)	2.0 sec., PHA events 1 spin, 2 min, Images
Sensitivity, G x ε (cm^2-sr)	~1.6 for O, ~0.3 for H
G x ε for 3° x 3° Pixel (image accumulation bin)	.0027, tapered at FOV edges
Pixel array dimensions*	4M x 8E x 40A x 120A
UV rejection	$<3 \times 10^{-7}$ (Ly-α, I below 10kR)
Electron rejection	$\sim 10^{-5}$ (E < collimator rejection)

Ion rejection	~10^{-5} (E < collimator rejection)
Dynamic range	~10^{7}

* E => energies, M => masses, A => angles

The magnesium deflector plates are serrated to inhibit forward scattering of incident particles. Commandable potentials of up to ±6 kV may be applied to alternate plates to sweep energetic charged particles with energies ≤ 500 keV/e into the plate walls (excluding them from the detector). Initially this potential will be limited to ±4 kV, and may be raised to the full value according to its stability in flight. The shielding effectiveness of the collimator has been measured in the laboratory (Figure 5) and is adequate to permit neutral particle imaging below the sweeping energy even while the instrument is within moderate magnetospheric plasma environments.

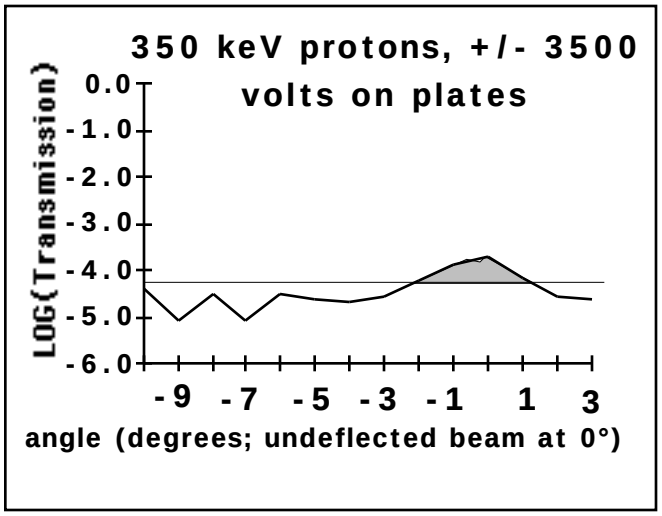

Figure 5 Accelerator test of deflector ion sweeping at an intermediate voltage, indicating charged particle rejection at better than 4 orders of magnitude. The peak with shading is in the position of the undeflected beam, and results from energetic neutrals created via charge exchange of energetic ions in the beam tube.

2.1.1 *Measurement Technique*

An incoming neutral particle encounters and penetrates a thin foil, producing secondary electrons (Figure 4). The secondary electrons are first accelerated perpendicular to the entrance foil by the E-field which is locally normal to the equipotential surface of the foil, and then steered electrostatically (using a combination of wires and shaped electrodes at fixed potentials) onto a start MCP with 1-D position sensitive anode. In addition to the entrance slit position, a start timing pulse taken from the start MCP is generated by this event. The original incident particle, after some angular scattering in the front foil, continues through the instrument, striking either (1) a second foil just in front of the stop MCP assembly, or (2) a position sensitive SSD.

In case (1), secondary electrons produced on the exit surface of the second foil are accelerated into the stop MCP with its 2-D imaging anode, mapping the position of impact and registering the stop timing pulse for the TOF measurement. In addition to this TOF and trajectory measurement, secondary electrons produced as the ENA enters the back foil are electrostatically accelerated and guided to the coincidence/SSD stop MCP (C/S MCP) (see Fig. 4). From the back foil to the , the electron travel time for these back-scattered electrons is constrained to < 40 ns by the steering potentials. The pulse generated in the coincidence plate is used in the valid event logic circuitry as a coincidence check on the MCP measurement, further reducing the probability that uncorrelated background is falsely counted as a neutral.

In case (2), the neutral strikes a pixel of the SSD, yielding both position (pixel ID) and energy. Secondary electrons generated at the surface are accelerated into the C/S MCP, with a travel time between the SSD and the MCP of between 6 and 10 ns, depending on which row of SSD pixels is struck. The signal produced in the C/S MCP is corrected for the electron travel time, and used for the SSD TOF.

2.1.2 *Detectors*

HENA uses two types of detectors, MCPs and SSD. They are described here is some detail.

Each MPC assembly consists of two MCPs in chevron configuration. Each plate has a length-to-diameter ratio of 60:1. These plates are of the long-life variety provided by Galileo ElectroOptics. The long-life is required by the expected EUV fluence over the mission, which would demand each plate to produce several tenths of a coulomb/cm^2.

The start and back plane MCPs are backed by position sensitive anodes (wedge and strip type), as well as capacitively coupled timing anodes. The C/S MCP is backed by a timing anode only. Entrance slit and back plane positions, as well as start, stop, and coincidence (or SSD stop) pulses are passed to the fast logic board, where they are checked against valid event criteria. If all valid event conditions are met (e.g., start + stop + coincidence for the MCP side of the back plane, or start + stop + energy pulse for the SSD side of the back plane), the times and positions are digitized and passed on to the DPU for classification and binning into images.

The solid state detector (SSD) contains four separate wafers, each divided into 5 x 12 pixels. The resulting array has 10 x 24 pixels over an area of ~ 5 x 10 cm^2, and each pixel is ~ 0.4 cm square. The SSDs are provided by MICRON, and meet the HENA specifications for leakage current (<10nA), window thickness (<0.1µ), and minimum electronic threshold (< 7 keV). Calibration of the SSD system indicates that HENA has an energy resolution of ~7 keV which, at the worst, provides a $\Delta E/E$ at E = 30 keV of 0.25. This is to be compared with the mission requirement for $\Delta E/E$ of < 0.7. After the limiting factors of energy loss in the front foil, energy loss in the detector window, and the minimum practical energy threshold setting, 30 keV is the minimum proton energy which can be measured using the SSD system. Since this is also the minimum practical energy for magnetospheric imaging (see Section 2.1.5 below) in this sensor, there would be little gained should lower energies be measurable.

These detectors are bonded to a flex circuit, which carries the signals to a bank of 240 AMTEK A225 hybrid preamplifiers spread over 5 circuit boards. From there, the signals pass to a series of ASICs (Application Specific Integrated Circuits) which further amplify the signals, produce pixel IDs and digitize the pulse height. These ASICs also produce a strobe which alerts the HENA fast logic board to the event, and the information is passed on to be combined with the timing pulses from the start and SSD stop MCPs. If the fast logic board accepts the event as valid, it is passed to the DPU where it is binned into an

accumulating image. All electronics were designed to meet mission radiation requirements (see Appendix A, Section A-1.1.3).

2.1.3 *Mass Determination*

HENA can use two different approaches to determining the mass of an incident ENA. The primary mass determination is accomplished conventionally, by combining the SSD energy pulse and the TOF to determine the energy (= $1/2\ mv^2$) and velocity (v) of the ENA, and therefore its mass (m).

On the MCP side of the back plane, a different technique may be used for mass determination. The number of secondary electrons produced in each foil is dependent on the atomic number of the neutral atom; for the two most common neutral atoms expected, oxygen has been found to produce several times the number of secondaries that hydrogen will produce. Exploiting this phenomenon, we record the pulse-height of the MCP signal and determine the species based on that measurement.

This technique is the primary approach to mass determination on the Cassini INCA sensor, which has no SSD system. For HENA, it will only be used as a back-up capability, should the SSD system fail.

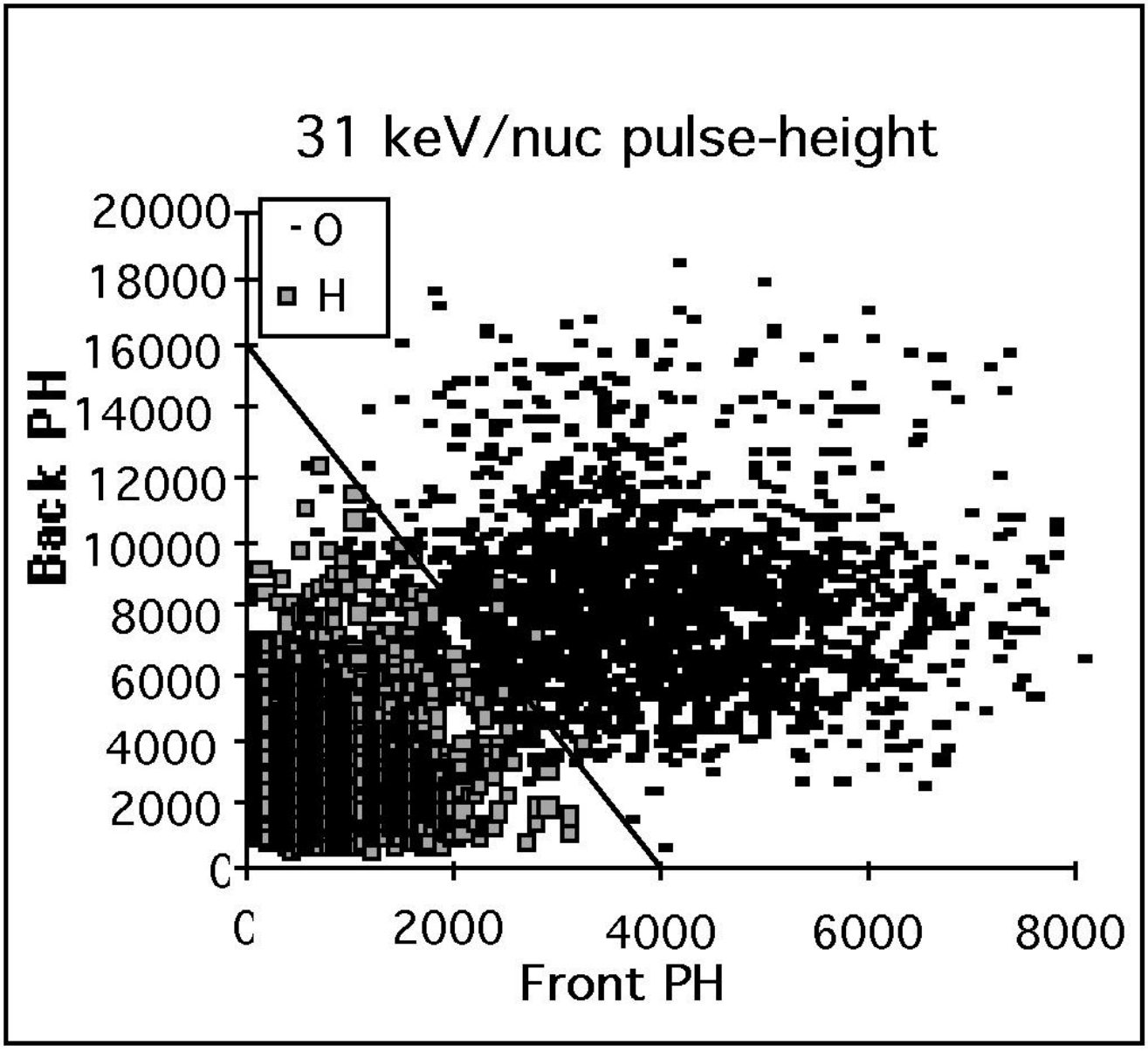

Figure 6. Separation of oxygen and hydrogen using MCP pulse-height signatures. The 31 keV O and H measurements are overplotted. The hydrogen separates as lower MCP pulse-heights. At higher energies, this separation becomes more complete. Data from calibration of Cassini/MIMI/INCA sensor (Mitchell *et al*., 1998).

2.1.4 *Foils and UV Sensitivity*

There are two thin foils in HENA, the Si-polyimide-C foil at the entrance slit and the C-polyimide-C foil at the back plane sensed by the 2-D MCP array. Both foils serve as the source of secondary electrons for the timing signals, one start and one stop, for the TOF analysis. The second foil also provides back-scattered electrons for the coincidence pulse. Electrons are also produced in the foils by photoionization

by vacuum ultraviolet light EUV and FUV, predominantly in the Ly-α line from the Earth's hydrogen geocorona. The foil must therefore be chosen thick enough to attenuate the Ly-α to an acceptable level, so that the position and TOF circuitry is not swamped by false counts. The TOF measurement is made by recording a start signal followed by a stop signal some time later. Any single photon can produce a start or a stop, but not both. As long as the time between a false Ly-α start and a separate false Ly−α stop is long compared with the maximum valid TOF period (~100 nsec), this background will not produce false events. The electronic design assumes nominal upper limits for Ly-α start events of $\leq 10^5$ secondary electrons per second, and for stop events ≤1000 secondary electrons per second. The Ly-α flux from the sunlit atmosphere at Earth (excluding the sun itself) is ~10 to 30 kR (Rairden et al., 1986), which corresponds to ~0.32 to 1.0 x 10^{10} photons/sec incident on the front foil (which has a ~4 cm^2-sr geometry factor). The forward photoelectron yield of a foil with a C exit surface by Ly-α photons is ~1% (Hsieh *et al.*, 1980). The HENA foil (provided by Luxel corporation of Friday Harbor, Washington; Powell, 1993; Powell *et al.*, 1990) comprises 3 layers. They are 6.5 μg cm^{-2} Si, 7.0 μg cm^{-2} polyimide, and 1.0 μg cm^{-2} C with a measured 1.5 x 10^{-3} Ly-α transmittance to reach a conservative design goal of ≤ 0.5 to 1.5 x 10^5 Ly-α induced secondary electrons per second when the brightest portion of the Earth's atmosphere/exosphere fills the FOV. The foil materials were selected based on the work of Hsieh *et al.*, 1991. Laboratory calibrations of the heritage INCA instrument have verified this system's capability to continue to image and reject Ly-α background at UV-induced counting rates in excess of 3 x 10^5 s^{-1}. The front foil is mounted on a 70 line/inch nickel mesh (82% transmission), supplied by Buckby-Mears. The stop foil, composed of 7.0 μg cm^{-2} of polyimide and 5.0 μg cm^{-2} carbon, will reduce the Ly-α flux to the back, 2-D imaging MCP by about another factor of 100. With the sun in view, because the quantum efficiencies for secondary electron production are so high at EUV wavelengths, no practical foil composition-thickness combination could be identified to sufficiently suppress it. We will operate a mechanical shutter once per spin, while the sun is in view, to avoid high rates (see discussion of shutter, Section 2.1.7).

2.1.5 *Angular Resolution*

The angles within the HENA FOV are defined in Fig. 7

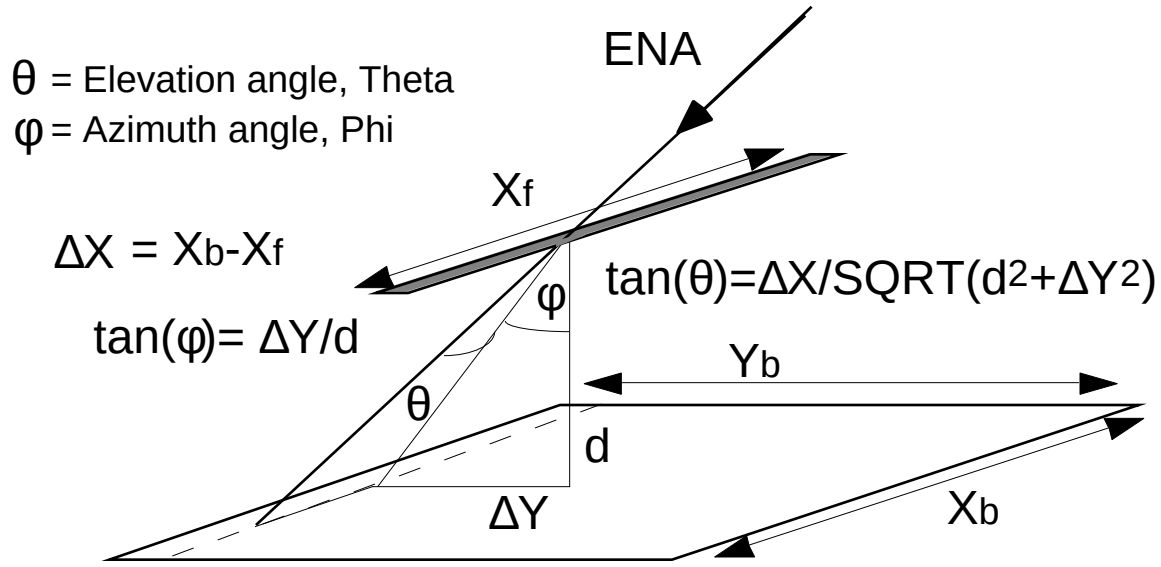

Figure 7 HENA elevation and azimuth angle definitions. Elevation angle changes parallel to the collimator fins. Azimuth changes across the fins. Spacecraft spin vector is parallel to X.

Each measured ENA is added to an accumulating ENA image, according to its species, velocity, and trajectory. A map of the sky is maintained in memory, and each particle is binned into the image pixel of that map according to the time of its detection. This is accomplished at millisecond timing, so that motion introduced smear is not an issue. Higher velocity images are binned at 3° resolution, while lower velocity images are binned at 6° resolution. In this way, images are sampled in bins of finer angular spacing than the intrinsic resolution of the instrument (over-sampled).

Angular scattering in the foils, along with the angular spread introduced in the electron optics, has been measured during accelerator tests of the complete engineering model HENA sensor. Calibration results will be discussed in greater detail below. Representative angular Full Width at Half Maximums (FWHM)

a)

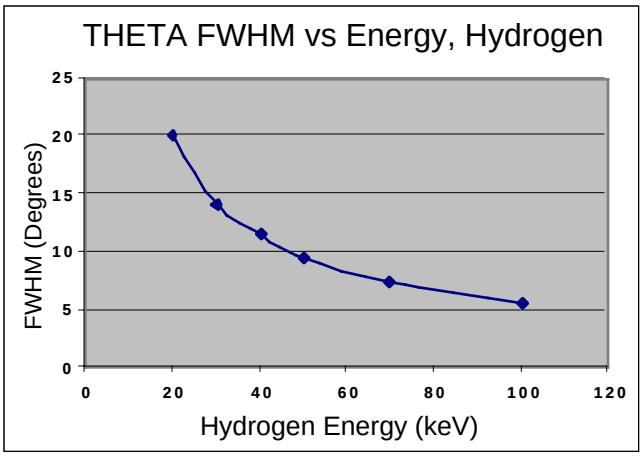

b)

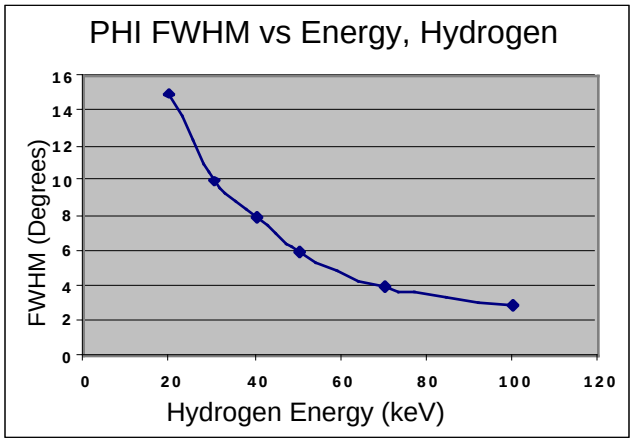

Figure 8 a) Elevation angle (θ) resolution vs hydrogen energy; *b)* Azimuth angle (φ) resolution vs hydrogen energy

measured on the MCP side of HENA are: for hydrogen at 100 keV, θ_{FWHM} ~ 5.25˚ to 6.0˚ and φ_{FWHM} ~ 2.5˚ to 4˚. For oxygen at 50 keV/nucleon, θ_{FWHM} ~ 5.0˚ to 7.0˚, φ_{FWHM} ~ 2.6˚ to 5˚. For helium at 90 keV (which is equivalent in velocity to hydrogen at 22.5 keV), θ_{FWHM} ~ 9.0˚ to 12.0˚ and φ_{FWHM} ~ 6˚ to 8. For hydrogen at 70 keV, θ_{FWHM} ~ 6.0˚ to 9.0˚ and φ_{FWHM} ~ 3.0˚ to 5.0˚. For hydrogen at 50 keV, θ_{FWHM} ~ 8.0˚ to 11.0˚ and φ_{FWHM} ~ 5.0˚ to 7.0˚. For hydrogen at 40 keV, θ_{FWHM} ~ 10.0˚ to 13.0˚ and φ_{FWHM} ~ 7.0˚ to 9.0˚. For the MCP back plane, the φ resolution is dominated by scattering in the front foil in all cases; the θ resolution is dominated by the scattering in the front foil and by the electron optics for the front foil imaging. The latter effect is dominant for hydrogen above about 60 keV, where the number of secondary electrons produced on average is ~1 and the scattering in the front foil is moderate. From 60 keV down to the lowest hydrogen energies imaged (about 20 keV), scattering in the front foil becomes increasingly dominant in the decrease in resolution. The position resolution achievable by the start electron optics is modeled in Figure 9. For the models, data from Meckbach *et al.* [1975] was used to represent the secondary electron energy spectrum. The figure suggests that for single secondary electrons, the spread in the start position has a full width/half max of ~2 to 4 mm. This is consistent with our calibration results for protons. For moderate proton energies, a fraction of the events will produce 2 or more secondaries; therefore, we may be able to create separate images selected on the basis of start anode pulse height, allowing for higher resolution to be achieved on the 2-or-more secondary electron events. This would have the effect of improving the FWHMs stated above for theta in a fraction of the >45 keV hydrogen by about 2°.

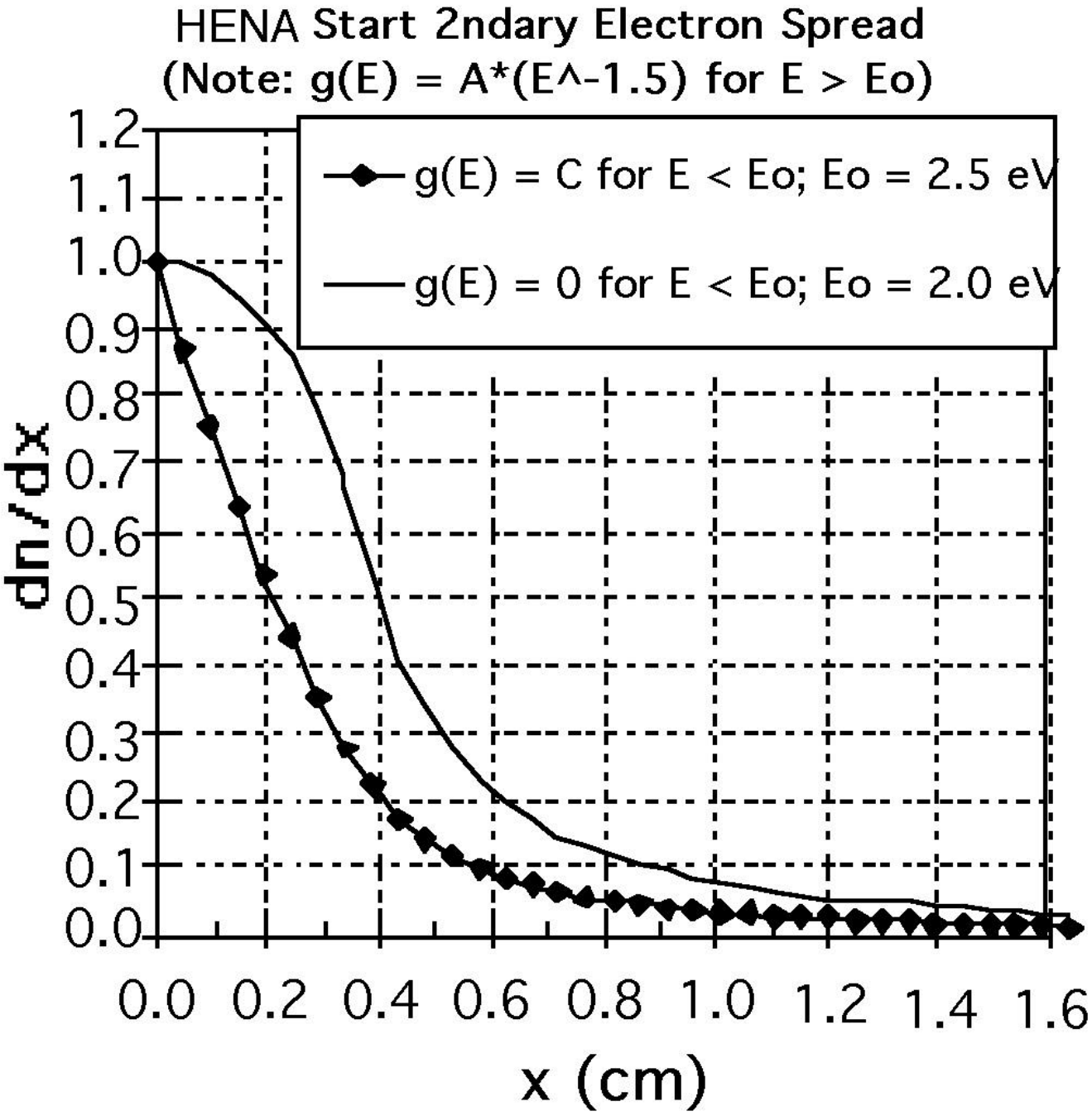

Figure 9. Model start position uncertainty due to random velocities of start secondary e^-.

For the SSD back plane, which shares the same start imaging assembly used by the MCP back plane, the image resolution is dominated by the start position resolution and the SSD pixel size at high energies (> 60 keV/nucleon) and by start resolution and scattering at lower energies. The highest resolution possible for the SSD back plane is limited by the SSD pixel size (~4mm x 4mm). This, combined with a best resolution of 2mm (slit width) x ~4mm (entrance resolution for oxygen) for the entrance position, yields ~3° x 4° FWHM ($\Delta\varphi\Delta\theta$) best case resolution, before scattering of ENAs in the front foil is factored in.

For hydrogen the best case numbers are degraded in the θ direction by the start electron optics, to ~3° x 6° FWHM.

The HENA angular resolution as revealed by calibration is generally responsive to the HENA measurement requirements (see Table 2.1-1). Typically, the φ angle meets or exceeds those requirements, while the θ angle meets or falls slightly short.

2.1.6 *Sensitivity and Background Rejection*

The HENA head relies upon valid time of flight (separate start and stop) measurements, as well as coincidence pulses to differentiate background from foreground events. EUV will produce secondary electrons, but not correlated start, stop, and coincidence pulses. In order to produce false events that appear valid, an EUV start must be followed by EUV (or other) stop and coincidence pulses within a valid timing window. Other sources of false signals may come from high energy penetrating > 2 MeV energetic electron fluxes, which should only become a significant background inside L = 5 to 6, as well as ion fluxes above the rejection cut-off energy of the deflector deflection plates. The latter are discriminated against by their TOF signatures (i.e., too fast to be valid neutrals below the cut-off), although we expect to be able to image neutrals up to ~1 MeV when the ambient energetic ion flux above the cut-off energy is sufficiently low. The expected environment will give foreground count rates ranging from ~10^3/s for the inner magnetosphere down to ~1/s at greater distances and quiet conditions.

The system has an intrinsic window for valid events of ~100ns, based on the maximum valid TOF for a ~50 keV oxygen (which is the slowest valid ENA expected to be analyzed), and the coincidence window is ~40ns. For the MCP side of the back plane, the background rate for false valid events from uncorrelated background rates will therefore be ~1 x 10^{-7} · ~4 x 10^{-8} · R_{start} · R_{stop} · $R_{coincidence}$, where R_{start} (R_{stop}, $R_{coincidence}$) is the uncorrelated singles rate due to penetrating background and EUV on the start (stop, coincidence) MCP. Thus the false valid event rate is ~4 x 10^{-15} · R_{start} · R_{stop} · $R_{coincidence}$, assuming the accidental rates are uncorrelated. For the EUV generated background rates expected with the measured foil transmittances, i.e. $R_{start} = R_{coincidence} \leq$ ~150,000 counts/sec and $R_{stop} \leq$ ~1500 counts/sec (see discussion in section 1.3, above), the maximum false coincidence rate attributable to EUV will be ~1.0 events per second in regions with low foreground rates. If a penetrator hits both MCP's, and produces a correlated pulse pair, the probability of a false coincidence event being registered goes up. However, by requiring a minimum TOF of about 6 ns (corresponding to a 400 keV proton TOF), we will discriminate against some of these very fast particles in regions where they might otherwise dominate the signal. Using the coincidence requirements, background rates from penetrators (cosmic rays and magnetospheric energetic particles) combined with uncorrelated EUV accidental rates are expected to be <0.1 per second at apogee, increasing as IMAGE enters the penetrating > 2 MeV electron flux in the inner magnetosphere. To the extent that we are able to discriminate against EUV and high energy particles (which also tend to produce only one secondary electron at a time), we can further reduce sources of background counts.

For the SSD side of the back plane, the combination of TOF window and SSD event pulse width (~10 μsec), along with the insensitivity of the SSD to EUV light, may result in even better background rejection. This number will be tunable, according to the minimum SSD threshold used (which will influence the EUV induced counting rate of the SSD).

2.1.7 *Sunlight and the HENA Shutter Operation.*

As the IMAGE spacecraft spins with its axis to the orbit plane, the HENA FOV is subjected to direct sunlight for 1/4 of each spin (30 seconds), for over half of the mission. While the foils and timing circuitry are designed to suppress background events caused by EUV light, both the intensity and the wavelength of solar EUV are far beyond the range where these techniques are effective. Therefore, the HENA design includes a fast actuating shutter (Figure 10), which is designed to be closed in approximately 1 second just before the sun enters the FOV, and reopened just after the sun leaves the FOV. Data accumulated as the shutter is moving will be ignored in analysis.

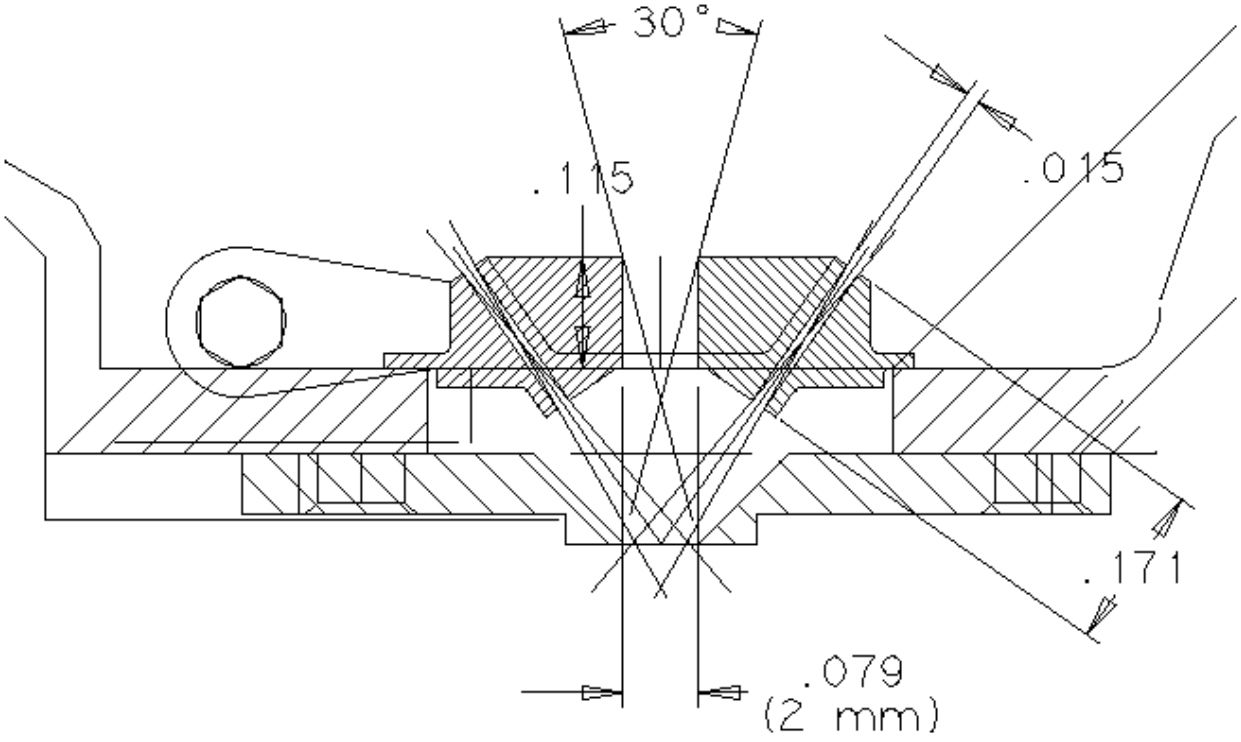
30°
.115
.015
.171
.079
(2 mm)

Figure 10 (a) HENA shutter, cross-section. Shown are the two open slits, which reduce the FOV to the back plane MCP and SSD detectors, as well as the pinhole, which is covered by an additional 300 nm thick foil, sufficient to reduce the solar EUV to a manageable level. The "pinhole" is actually a rectangular opening, with a 90° x 30° clear FOV (when in place over the entrance slit). Hex in pivot arm holes provide positive engagement with motor drive shaft (not shown).

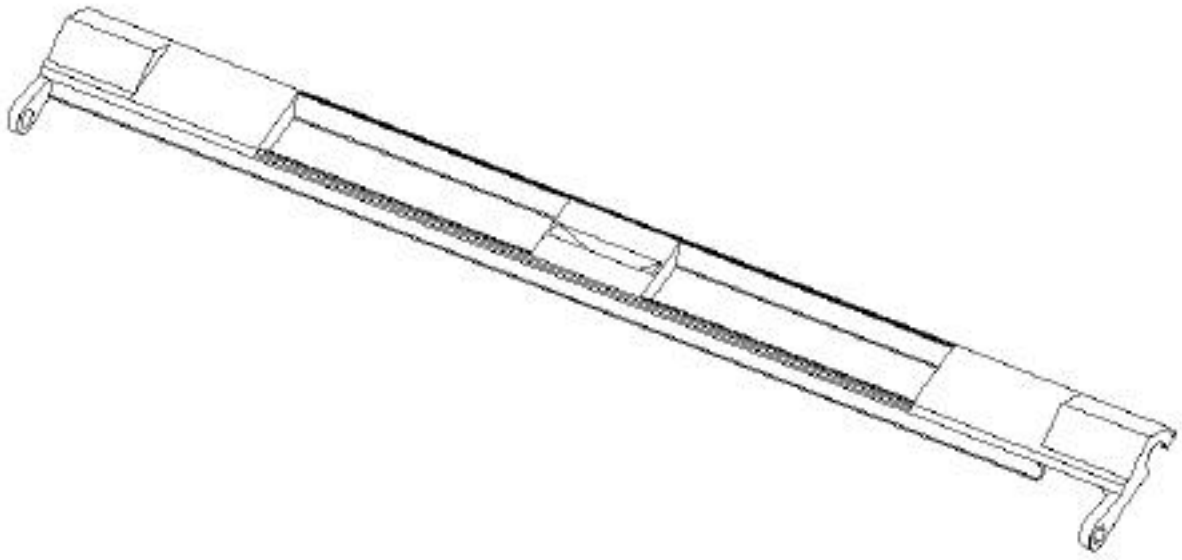

Figure 10(b) HENA shutter, perspective drawing.

The shutter is not strictly opaque, however. It was designed with 2 collimating slits, each of which passes ENA (or EUV) within a ~10° acceptance angle (in φ). One slit is positioned such that transmitted particles strike the back plane MCP along a specific band, while the other slit similarly passes particles which strike a band along the tilted portion of the SSD back plane. Thus, as HENA sweeps through the quadrant of its spin containing the sun, it can still accept ENA in both back plane sensors with reduced sensitivity. In addition, very high energy particles can enter through the pinhole, striking the central portions of both the SSD and the MCP. Twice within this quadrant, for 10° swaths, the sunlight is expected to enter the slits and effectively blind the sensor.

This shutter mechanism has been life tested, and is designed to be able to operate continuously throughout the 2 year mission. It also includes a failsafe mechanism, which consists of a spring that is to be cocked in flight after launch, and can be released at any time on command to force the shutter into the open position, should the motor actuator fail. Should the shutter spring fail to latch, the shutter can still be used, but will require more power (~1 watt, average) for the motor to drive and hold the shutter closed against the sprig force.

2.2 PROCESSING

The analog electronics amplifies the MCP and SSD detector outputs, processes the signals, converts them to digital words, and sends them to the Data Processing Unit (DPU) for analysis. This analysis derives the mass, direction, and count rates of the particles entering the sensors. The DPU then increments the appropriate rate elements in the counting memory, and stores the mass, velocity, and direction data in a FIFO buffer. The processor uses the data in this buffer to generate both the image planes and high resolution event words. The DPU then performs telemetry formatting, command processing, control I/O, and alarmed housekeeping functions.

The DPU controls power switching for the sensor head electronics. The DPU also controls the high voltage power supplies (HVPS) to alter the voltages to the sensor head as needed; several safety features implemented in the software protect the sensor from erroneous HV commanding.

The DPU collects data from the sensor head through the analog and fast digital logic electronics. Analog signals from the sensor head travel over coax cable to the main electronics unit (MEU), which houses the analog electronics, fast logic electronics, low voltage supplies, and the DPU. The signals are digitized to 14 bits resolution, processed by the analog electronics (valid event determination, pulse-height analysis, TOF, etc.) and sent to the DPU. The DPU also monitors instrument analog and digital status via housekeeping (HK) circuitry in the analog section of the MEU, and sets HV supplies and analog event threshold settings to selected levels.

2.2.1 *HENA Analog Processing.*

Figure 11 shows a block diagram of the HENA analog processing electronics. The HENA sensor generates an MCP "start" signal, an MCP "stop" signal, and MCP/SSD position and energy signals. The timing signals are processed in the Time-to-Digital Converter (TDC) circuitry (see Paschalidis, 1998; Paschalidis et al., 1998) over the range of ~6 to ~100 nsec with total system resolution of ~1.0 nsec. The TDC processing time is ~10 µsec. Position measurements are derived from the "start" and "stop" MCP anode signals and the SSD pixel ID circuitry. The pulse-height, timing and angle information from a valid event is latched into an event register where it is stored until the DPU is ready to process it.

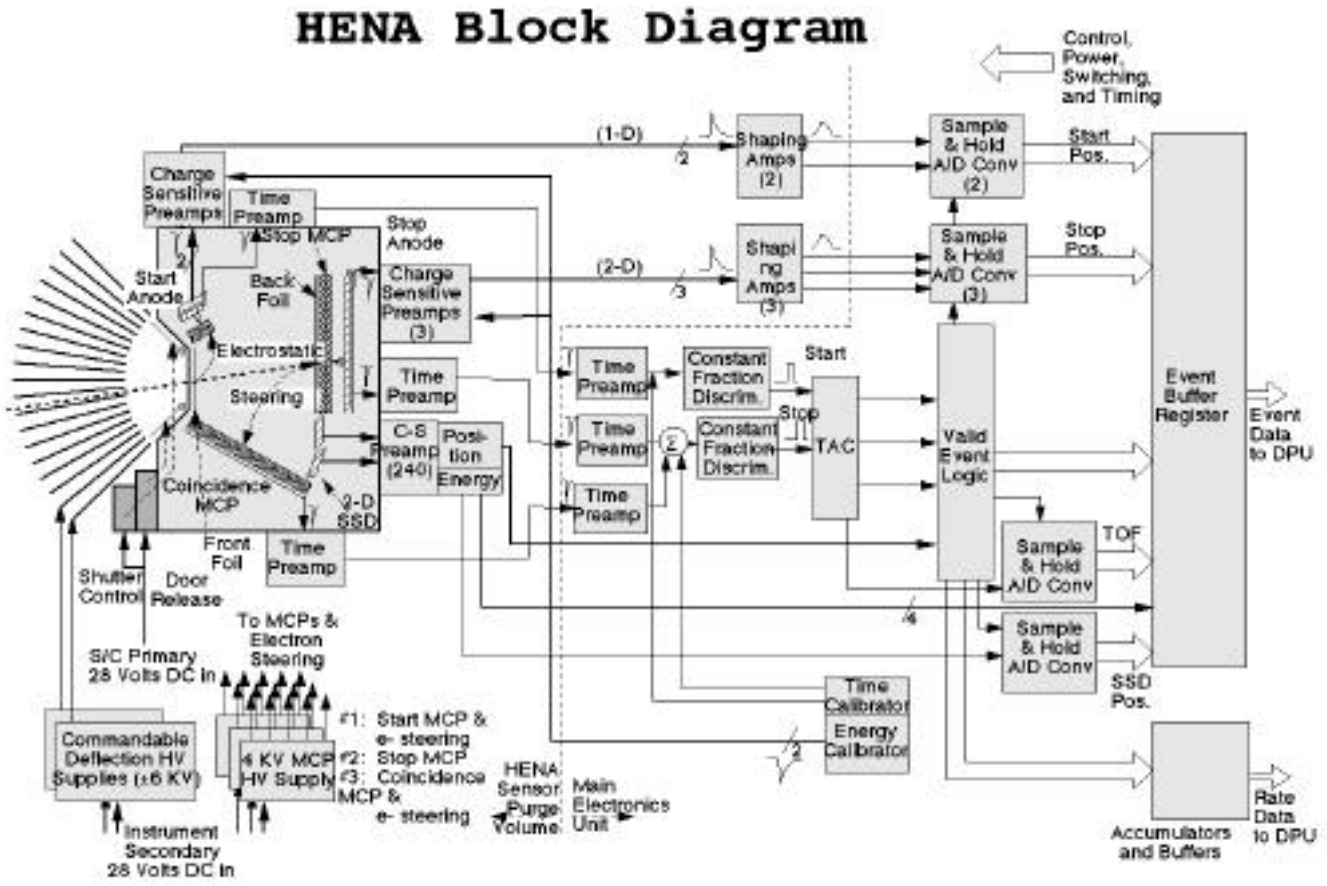

Figure 11. HENA sensor block diagram

2.2.2 *High Voltage*

Chevron stacks of two MCPs require high bias voltages extending up to about 3500 volts to operate properly. The current is drawn is < 60 μA. These bias voltages are commandable to adjust the gain of the MCP devices, thus correcting any gain shifts due to aging, burn-in, radiation effects, etc. The HENA sensor contains three MCP HV supplies, one to bias the start MCP, one to bias the coincidence MCP, and the third for the stop MCP. The secondary electron steering elements use voltages provided by these same supplies. HENA will also have similar high voltage supplies to bias the charged particle deflection plates. These supplies are also commandable, such that the deflection plate voltages can be varied between a low voltage and about 6 kV. Typically, they are operated at about ± 4 kV.

2.2.3 *Software Description*

The HENA DPU is closely derived from the Cassini MIMI DPU (the processor boards are identical), and the flight code designed for MIMI directly provided ~70% of the flight code needed for HENA. HENA flight software uses the FORTH interpretive programming language. The microprocessor, the Harris RTX2010, is designed to run in FORTH, and the interpretive characteristic of the language permits efficient debugging and verification of flight code.

The HENA boot PROM contains the start-up flight code, while the main body of the HENA flight software is downloaded from EEPROM into SRAM. Some parameter tables are downloaded directly from EEPROM into SRAM, but most are calculated at boot using parameters stored in EEPROM. Since the HENA DPU stores its flight software in on-board EEPROM, no instrument software load is nominally required from the spacecraft on power-up. New software code (or parameters) can be uploaded, if necessary, using the normal instrument command interface.

The DPU processing is primarily interrupt-driven; most processor time is spent analyzing the event data from the sensor, creating the ENA images, and formatting telemetry. The DPU is able to fully analyze approximately 6000 ENA events/sec. Telemetry production is closely monitored by the DPU to insure full utilization of the HENA allocation. The DPU monitors the spacecraft spin vector and phase to determine when the sun and Earth will fall within the sensor's FOV. Configurable by command, the DPU may close the shutter and/or lower the HV levels temporarily during these two conditions to avoid saturating the sensor front end circuitry.

The Housekeeping, alarm monitoring command processing, and instrument control functions require little processor resources, but have the highest priority. The DPU bulk SRAM memory is EDAC protected and scrubbed by the processor using spare processor time.

Time-tagged commands are passed to the HENA DPU by the Central Instrument Data Processor (CIDP) per the master sequence constructed on the ground. Commands are executed upon receipt, unless specific delays are included. Instrument macros may be stored in reserved memory, and subsequently used to execute a particular sequence of commands within HENA. Such macros are triggered by the CIDP.

2.2.4 *Operational Modes*

HENA has several operational modes:

--*Standard operational mode* (Normal Power, see HENA State Transition Diagram), produces all-sky images as output, parametrized by species, TOF as well as PHA data.
--*High Power Mode*, in which the HENA acoustic cover latch wax actuator release is powered. This operation, performed only once at the beginning of the mission, enables subsequent use of the shutter mechanism.
–*Calibration Mode*, which activates the HENA electronic calibrator(s).
--*Power On Reset*, which initializes the instrument hardware.
--*Sleep*, a mode in which HENA is in a low power stand-by state, with HV supplies remaining on, so that HENA may resume normal operations quickly.
--*2 Reserved States* for special circumstances when, for whatever reason, it is decided to separately disable either the SSD detector matrix, or the back-plane MCP.

The sensor will normally be ON throughout the mission. The collection of MCP-based and SSD-based images is simultaneous. HENA will be nominally run in neutral mode (collimator plates run at high voltage); ion mode is entered when collimator plate voltages are lowered to near zero volts, or turned off. Modes may be switched by command. The geometry factor may be varied by closing the shutter mechanism by command. The shutter will normally be left open, except for its use in sunlight mitigation. Decontamination heaters on the sensor will be used in early mission phases to facilitate outgassing.

Mode Description:

Normal Power: This is the normal operating mode for the instrument. All electronic subsystems are active except for the energy and time electronic calibrators. The shutter will nominally be closed and reopened once per orbit; the shutter requires less than one second to complete its movement in either direction.

Calibration: This is the same as the Normal Power mode, except that the energy and time calibrators are active.

High Power: This is the same as the Normal Power mode, except that the acoustic cover latch release wax actuator is powered; this mode is designed primarily for use during the period when the acoustic cover is being released, and when the shutter fail-safe spring is being latched. The wax actuator works on the same principal as an automobile thermostat. A heater warms the wax which expands, pushing a latch mechanism and unlatching a hinged, spring-loaded cover which seals over the fragile foil in the entrance slit, protecting it from acoustic energy during launch.

Sleep: This mode is defined to allow the HENA instrument power to be reduced while avoiding power cycling critical subsystems such as the high voltage supplies. The sensor amplifier circuitry, shutter power, and heaters are turned off, but the MEU housekeeping electronics and the analog processing are fully active. This preserves the software configuration information in the DPU, alleviating the need to reload parameters, etc. when the Normal Power mode is reactivated.

Power On Reset This is a 'safe' mode, the mode into which the instrument boots up. It is designed to put the instrument into an alive but quiescent state, from which it may be commanded into any of its operational states.

SSD on, MCP off This state may be used in ground test, as well as in flight, under special circumstances when the MCP side of the back plane is not desired.

SSD off, MCP on This state may be used in ground test, as well as in flight, under special circumstances when the SSD side of the back plane is not desired.

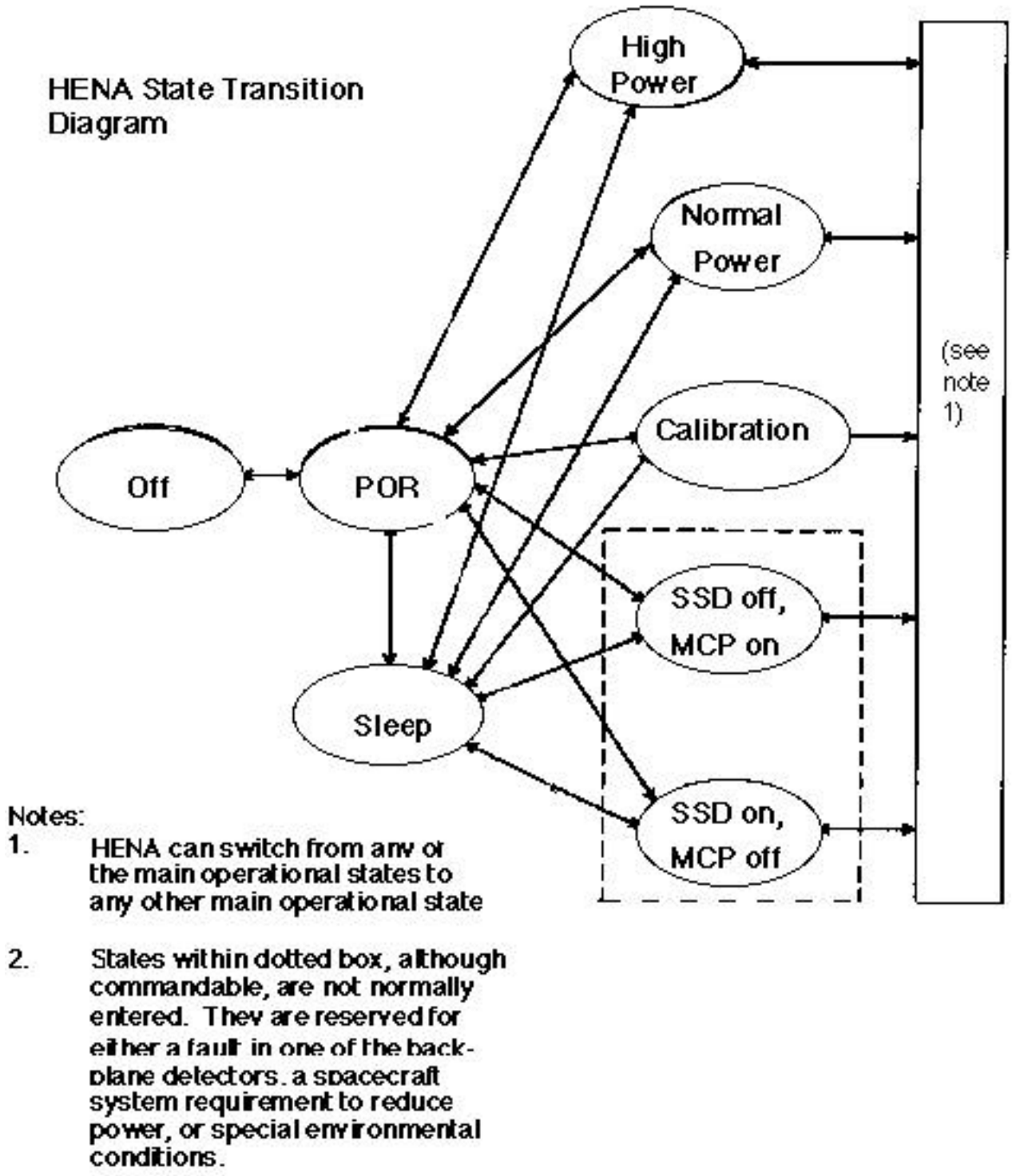

Figure 12. HENA State Transition Diagram

2.3 OPERATIONAL CONCEPTS

2.3.1 *Ground Operations*

Ground Operations will be conducted by Internet link to the GSFC Science Mission Operations Center (SMOC). After appropriate review process at the HENA Team and Project levels, commands will be sequenced using the HENA GSE software, sent electronically to the GSFC Operations Center, confirmed, and radiated to the spacecraft. Downlink data will be reviewed daily for health and safety, and science data will be distributed by the SMOC on DVD for routine processing, analysis, and selective conversion to higher level data products. Level 1 Browse products will be maintained on the SMOC website.

2.3.2 *On Orbit Operations and Testing*

Early on-orbit operations will include real-time commanding for initial turn-on, acoustic door release, and high voltage ramp-up. Nominal operations will include infrequent (~1 per week) uploads of parameters and/or patches to flight code. Anomaly response will also rely upon real-time commanding, when required.

3. Calibration

Calibrations of the HENA sensor were conducted at the Goddard Space Flight Center Van deGraff facility. The sensor was mounted on an articulation mechanism (Fig 13a and b) within a 36 inch diameter vacuum chamber. This mechanism provided full beam coverage in angle and position on the HENA detectors. Oxygen, nitrogen, helium, and hydrogen were accelerated to energies from 10 to 200 keV/nucleon, and the HENA angular and energy response was recorded. Below, we provide samples of some of the calibration data, after analysis. The data is presented in two sections, 3.1 for the MCP back plane, and 3.2 for the solid state detector back plane.

a) 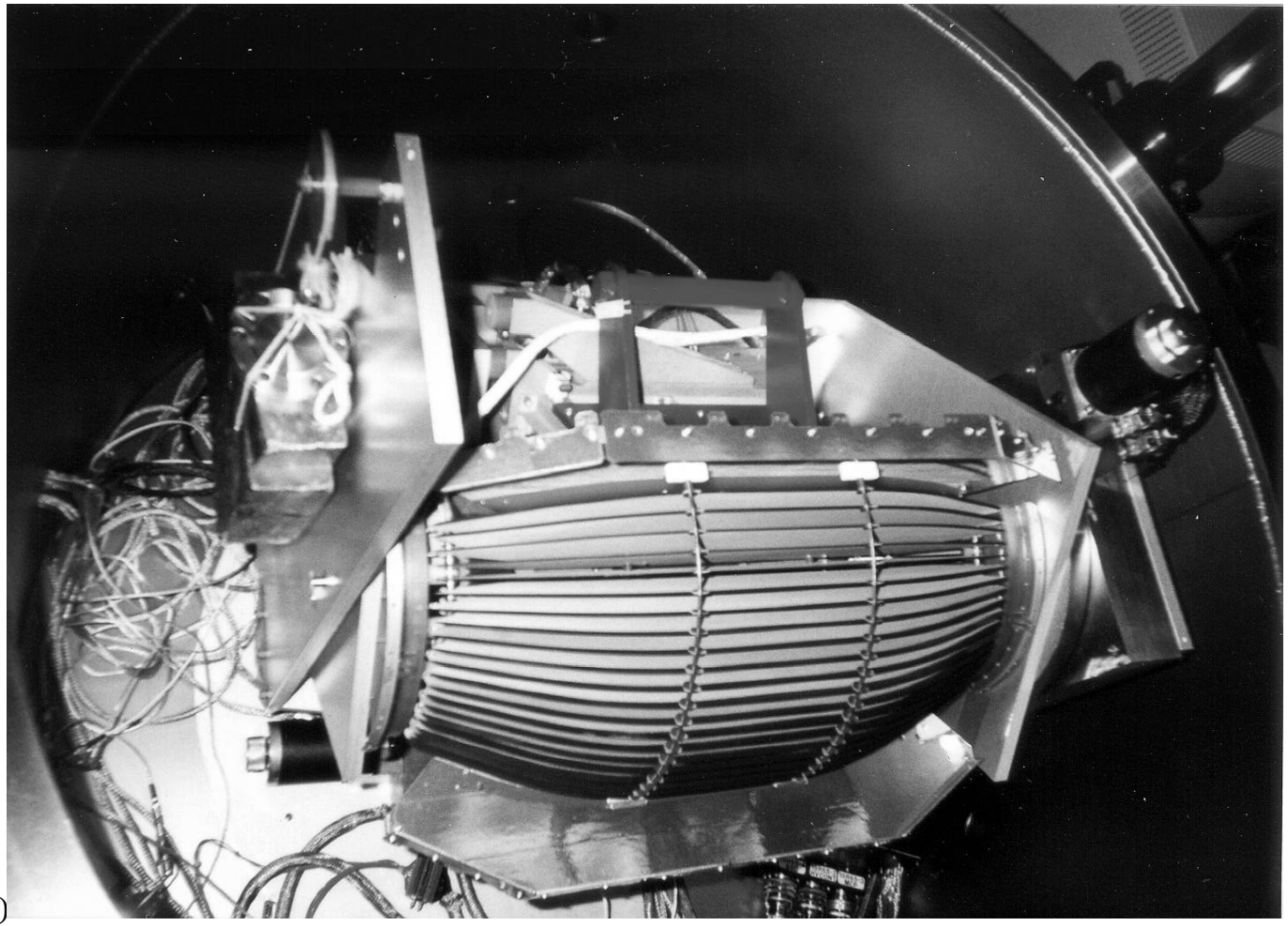

b) 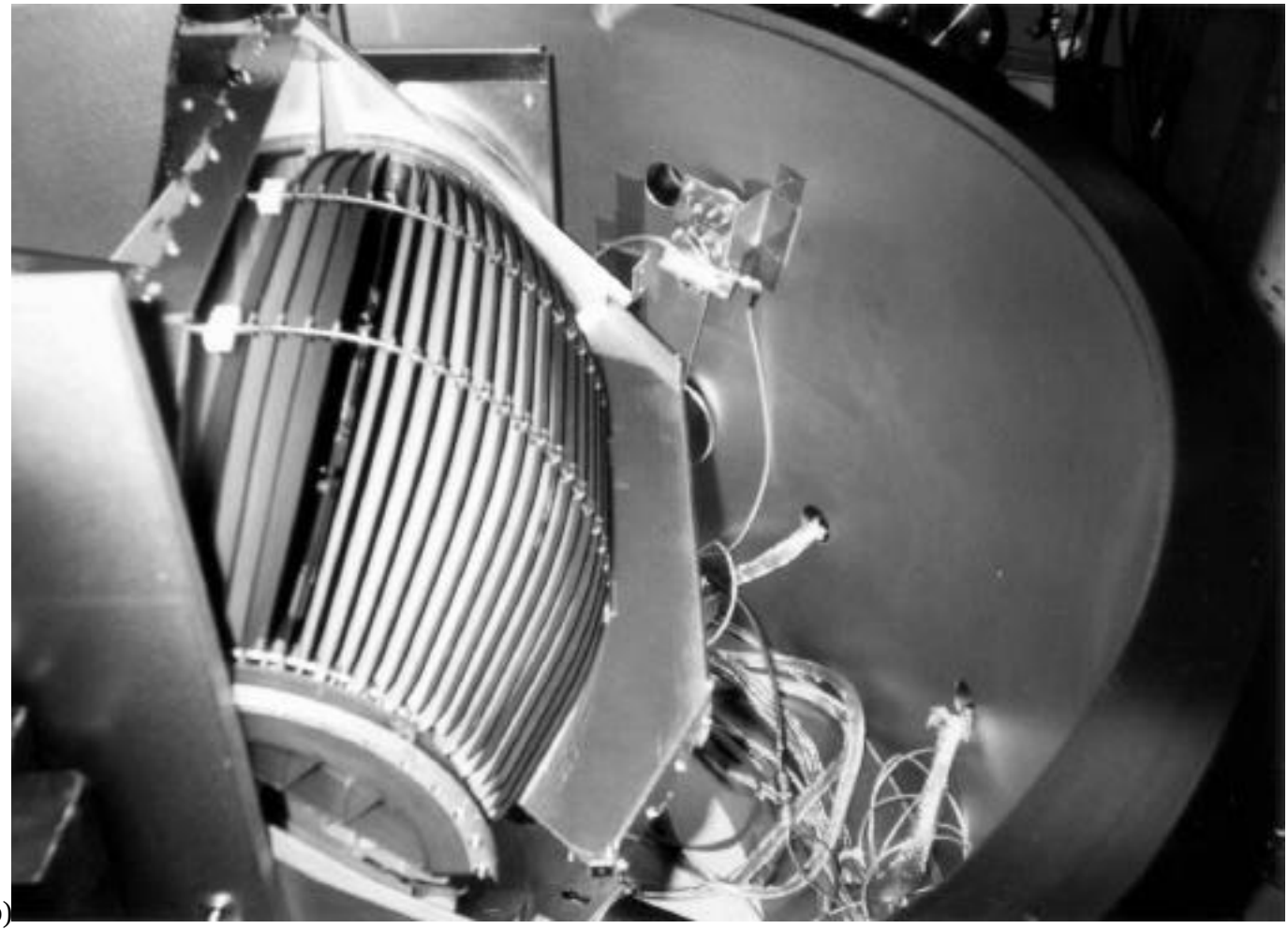

Figure 13 a) HENA sensor mounted on articulation mechanism, in chamber. *b)* View of calibration setup showing beam tube opening (upper center).

3.1 MCP BACK PLANE

The MCP back plane was tested at several hydrogen energies, as well as an extensive angular survey at one oxygen and one hydrogen energy. Data for the 800 keV (50 keV/nucleon) oxygen data are shown in Figure 14.

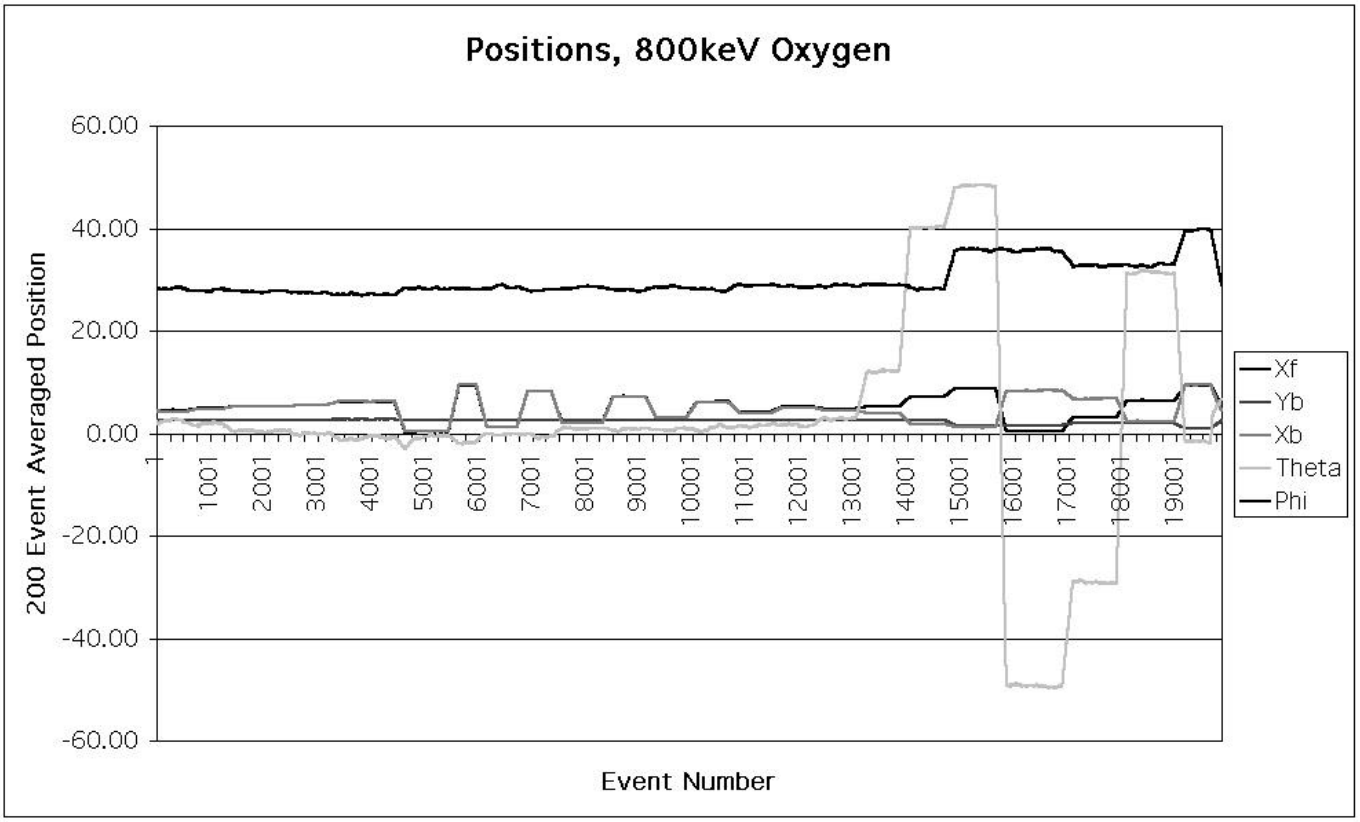

Figure 14 Traces of 200 particle running averages of the front foil position (Xf), back MCP position parallel to the front foil long axis (Xb), and the back MCP position perpendicular to the front foil (Yb). Also shown are the elevation angle (θ) and azimuth angle (φ)

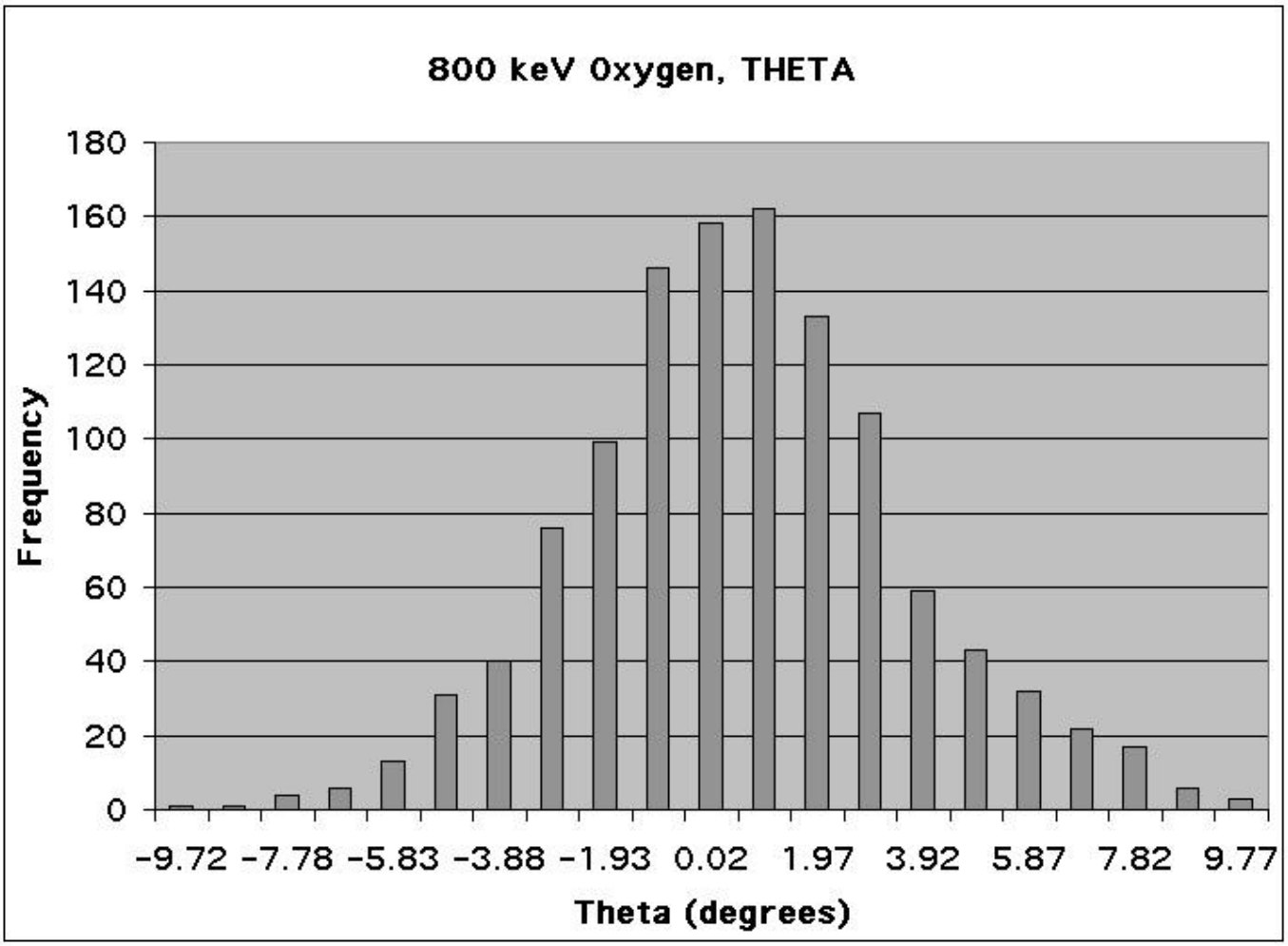
800 keV Oxygen, THETA
Frequency
180
160
140
120
100
80
60
40
20
0
-9.72 -7.78 -5.83 -3.88 -1.93 0.02 1.97 3.92 5.87 7.82 9.77
Theta (degrees)

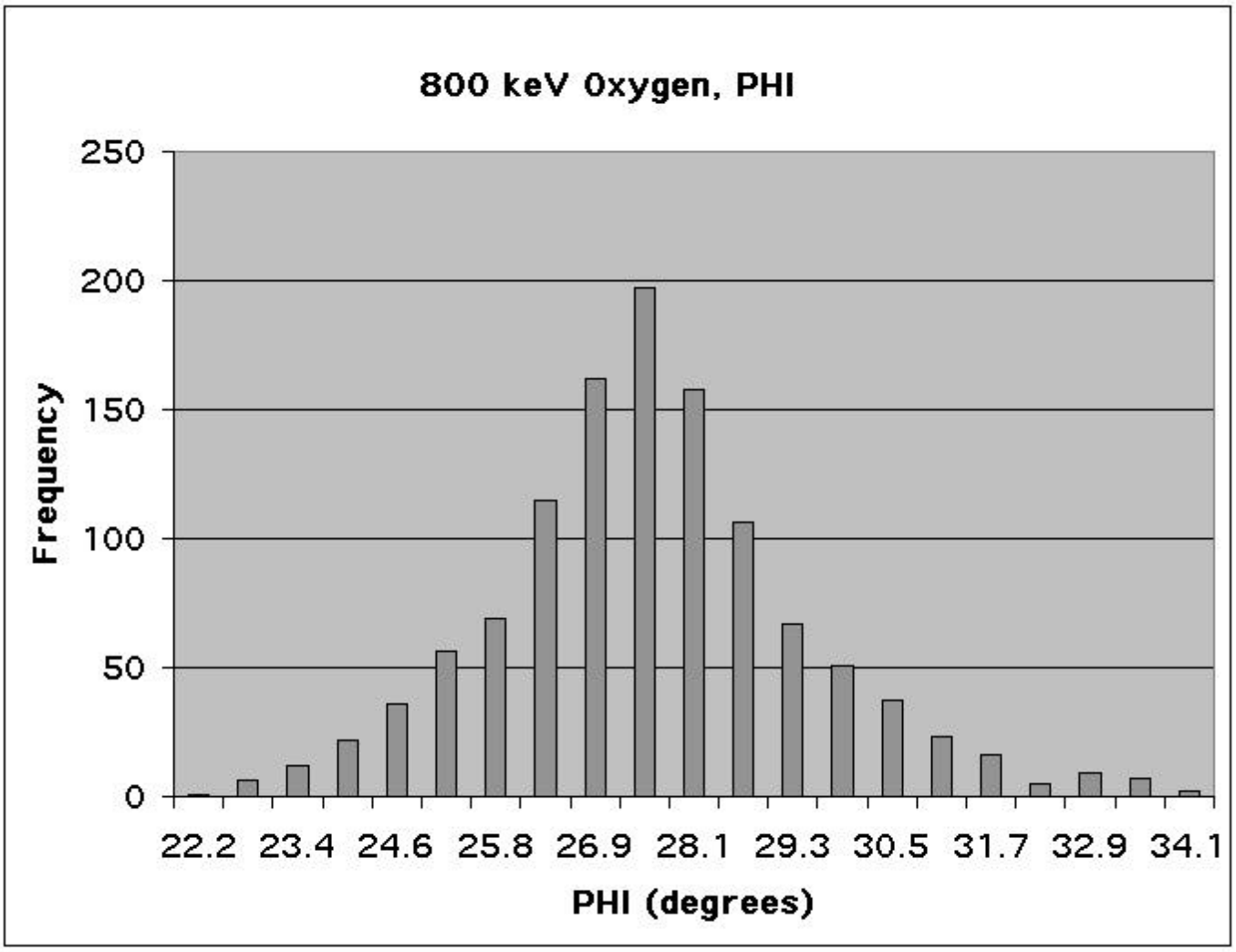

Figure 15 Histograms of θ and φ for 800 keV oxygen.

Histograms of the individual particle measurements for one choice of angles are shown in Fig. 15. These show that the FWHM for θ is ~5°, and for φ ~ 3.3°. In Fig 16, running averages of the FWHM for Xf, Xb, Yb, θ, and φ are shown. The FWHM for the angles vary somewhat as a function of position.

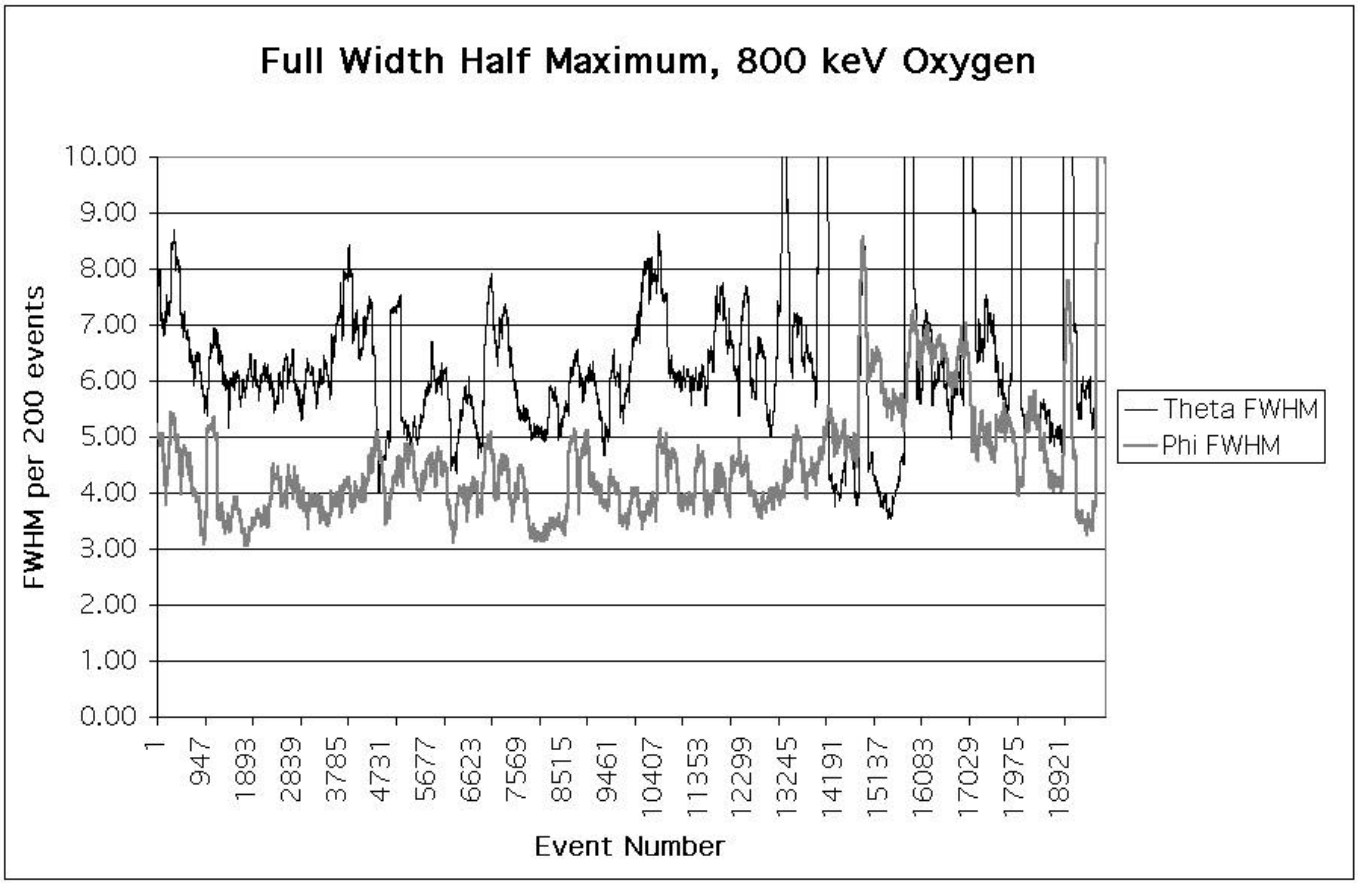

Figure 16 Running averages of FWHM of the values for Xf, Xb, Yb, θ, and φ, for 800 keV oxygen

Thorough measurements of the angular response to 100 keV hydrogen were also taken. The resolution characteristic of these measurements is summarized in Figures 17 and 18, below.

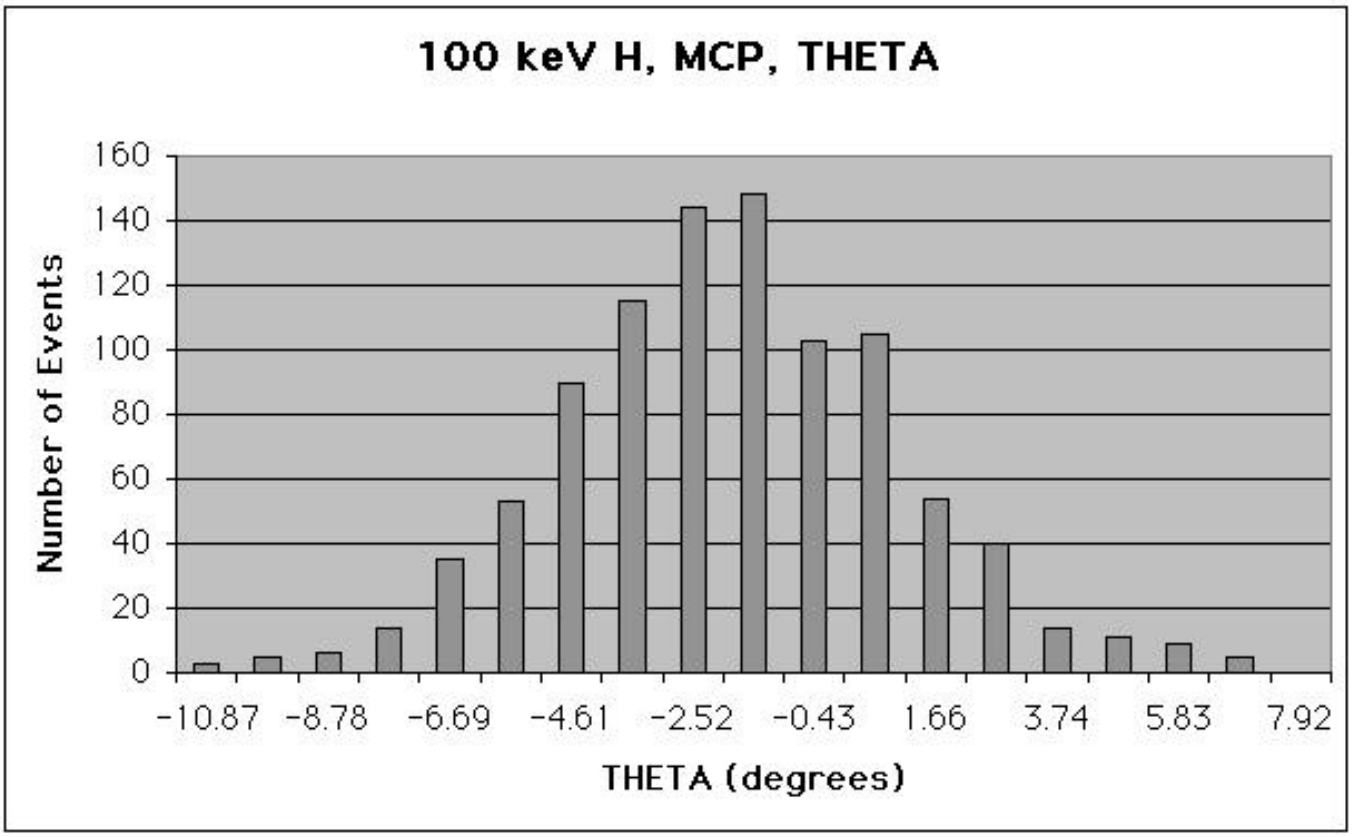

Figure 17 Histogram of θ for 100 keV hydrogen.

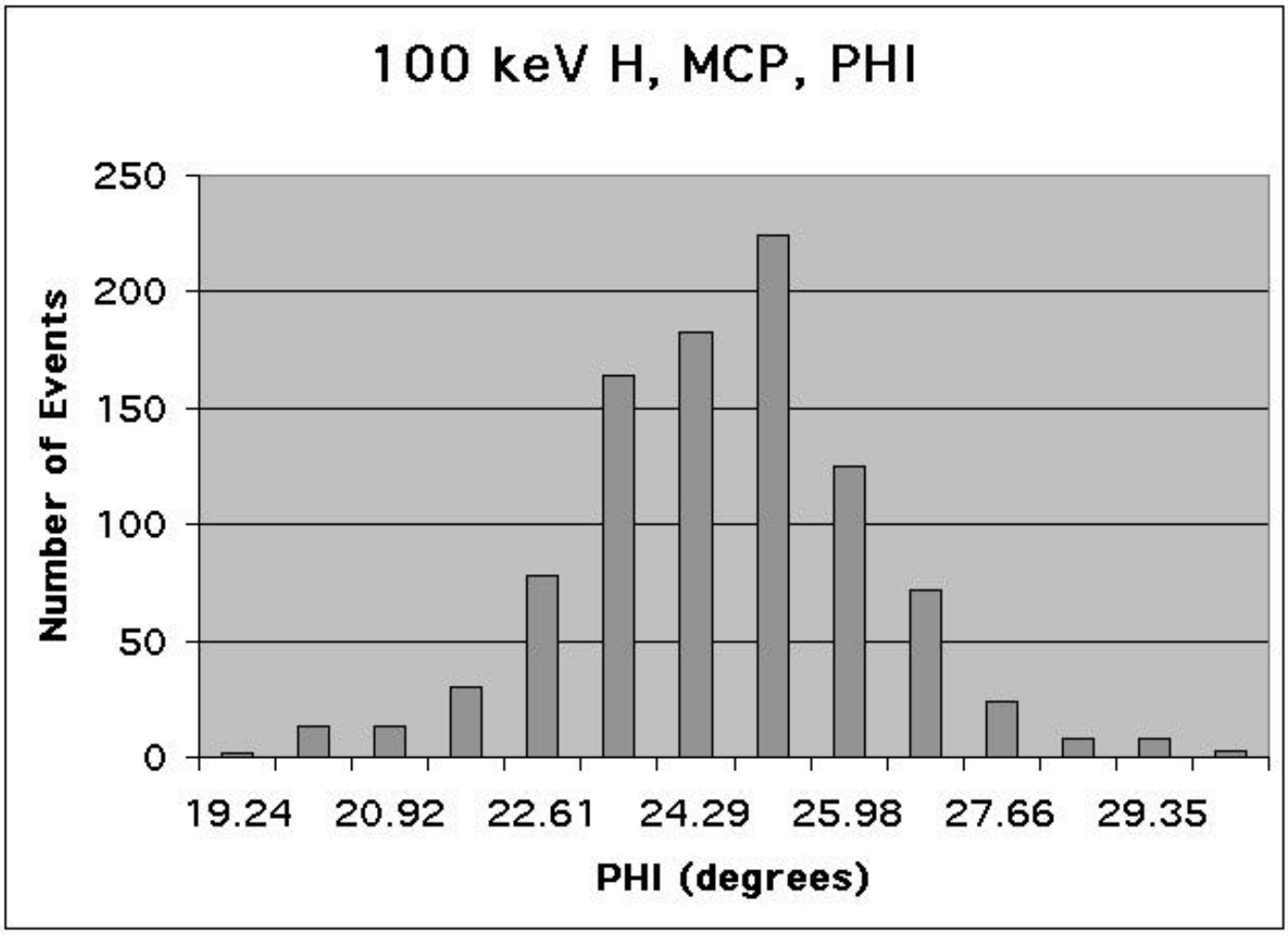

Figure 18 Histogram of φ for 100 keV hydrogen.

These figures show that the FWHM for 100 keV hydrogen is comparable to that for 800 keV oxygen. Dependence on energy is given in Fig. 8.

3.2 SSD BACK PLANE

The SSD side of the sensor was likewise tested at a variety of angles, energies, and species. Results for 100 keV hydrogen are presented below.

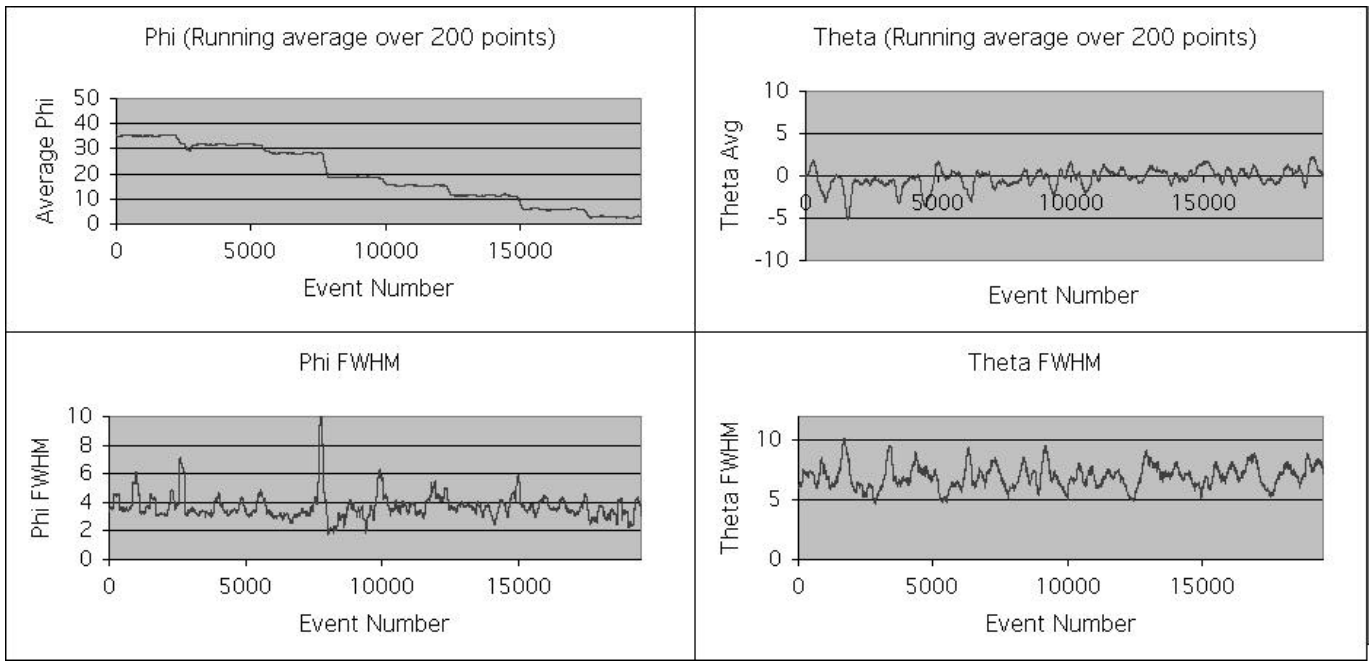

Figure 19 Summary of angular response of SSD images for 100 keV hydrogen. On the left, azimuth and FWHM for azimuth are given. On the right, the same quantities for elevation angle are shown.

The angular resolution for the SSD measurements is similar to that for the MCP measurements. For the SSD images, the limiting factors at this energy are the SSD pixel dimensions (4mm square), and the electron optics which smear the front foil position (see section 2.1.5).

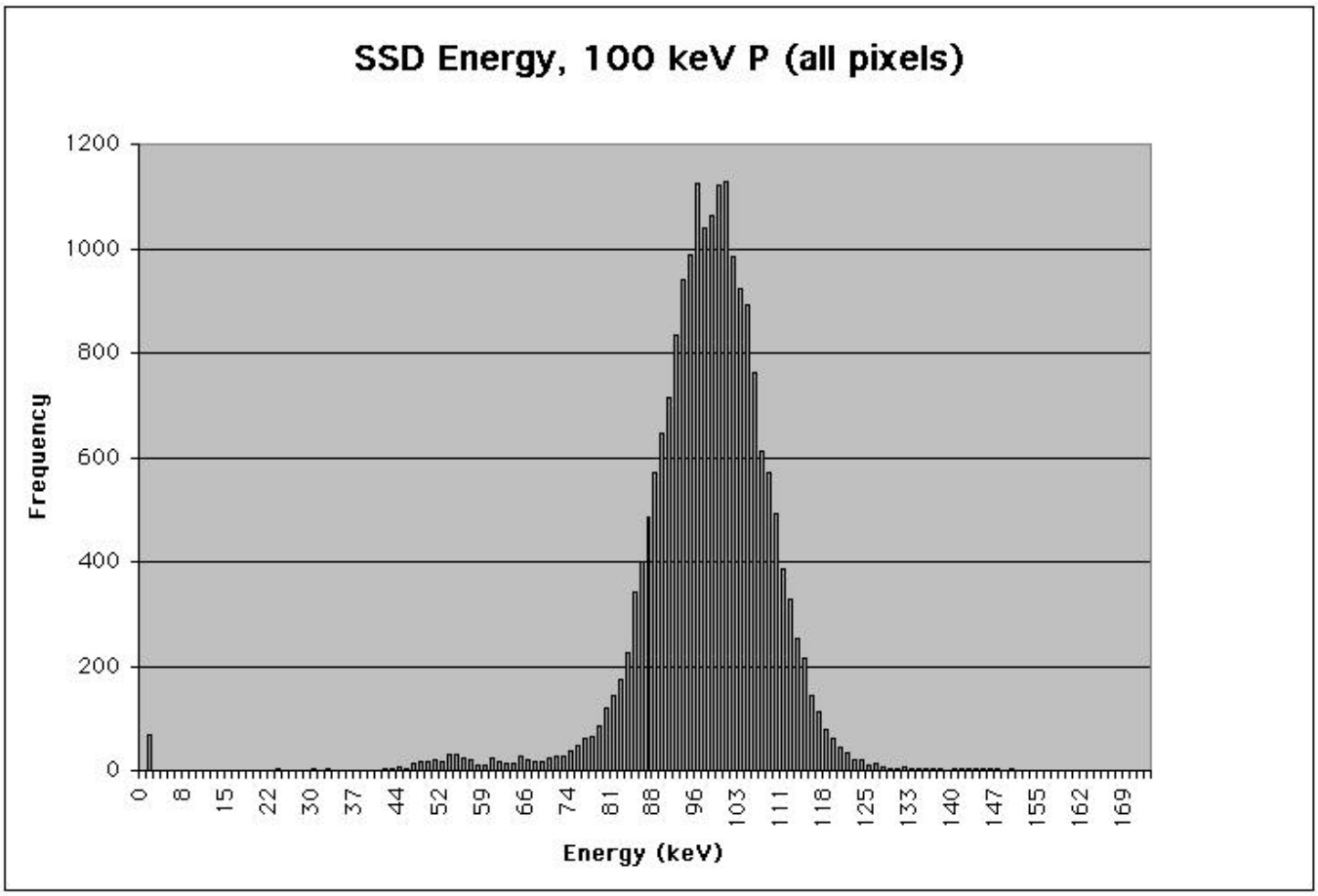

Figure 20 Energy histogram, over all SSD pixels.

In Fig. 20, a histogram of energy measurements for 100 keV hydrogen is shown. This includes measurements over all SSD pixels, with no adjustment for individual pixel calibrations. Individual pixels have histograms approximately half this width. Offsets may be applied to each pixel separately, so that the spread introduced by this variation will be removed in flight. (Although the calibration data exist to make this correction, it has not been applied as of this writing. However, even without correction the instrument will meet its mission level requirements for energy resolution.) Other features of note include a small low energy tail (ascribed to known pixels—these can be ignored by flight software), a peak at zero energy (also ignorable), and a very small high energy tail, which is contributed by only 3 pixels and can also be ignored.

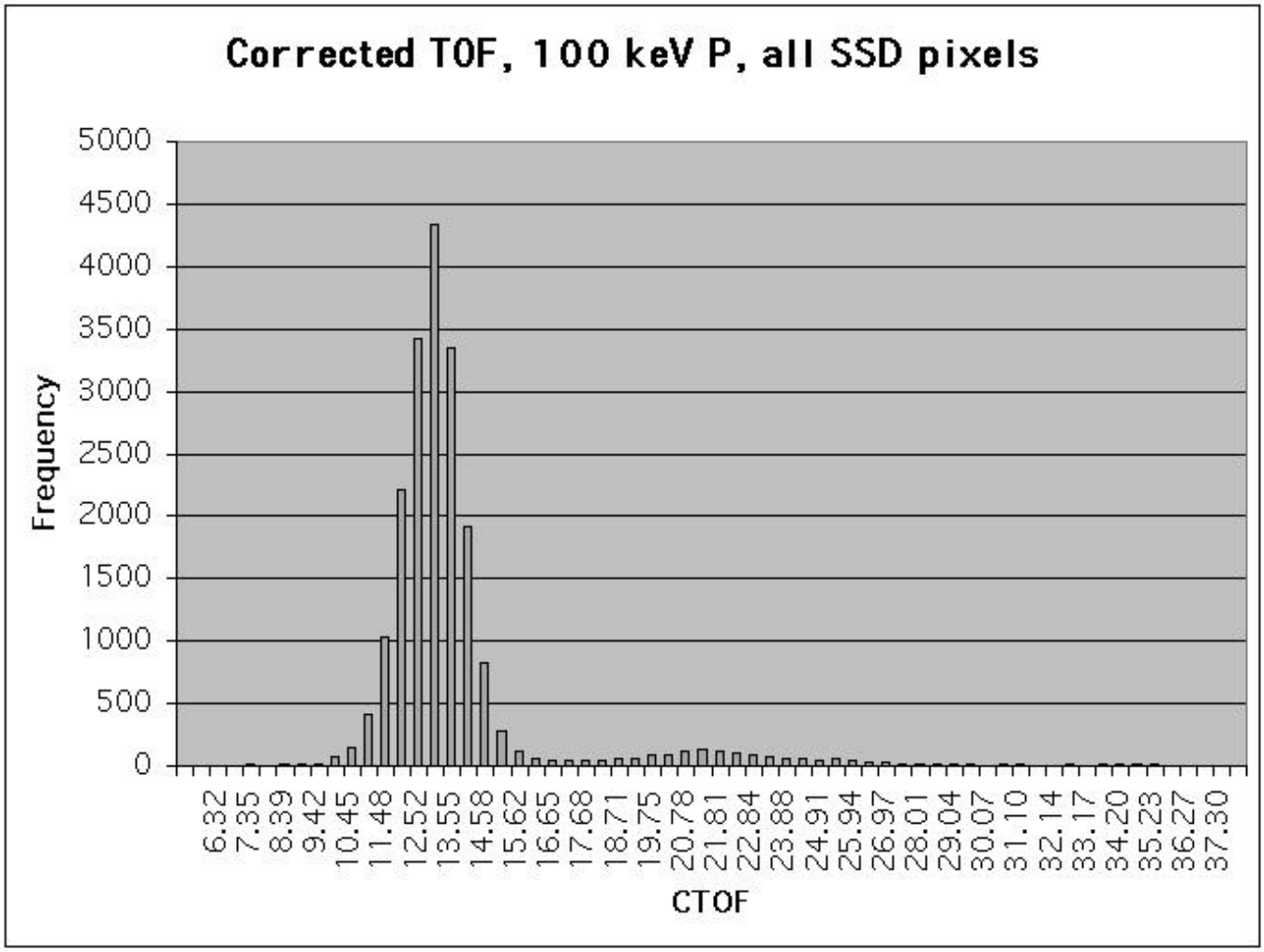

Figure 21 Histogram of measured times of flight for the SSD side of the sensor.

In Fig 21, we present a histogram of the corrected times of flight (CTOF) for the SSD side of the sensor. These TOFs are corrected for the ENA trajectory, as well as the stop secondary electron trajectory from the SSD surface to the SSD stop MCP. The main peak is ~1 ns FWHM. There is a secondary peak at ~ 21 ns. This peak results from a tendency for a small fraction of the secondary electrons to execute a "bounce" in their trajectory, which adds a discreet increment of ~ 8 ns to the measured time of flight. This population is primarily restricted to events at the outside edges of the SSD. If these pixels are eliminated from the measurement, the histogram in Fig 22 results. This histogram is plotted on a logarithmic scale, so that the residual tail can be seen more easily. In this case, there is no discreet peak at 21 ns, but rather a broad high TOF distribution all at least a factor of 300 below the main peak.

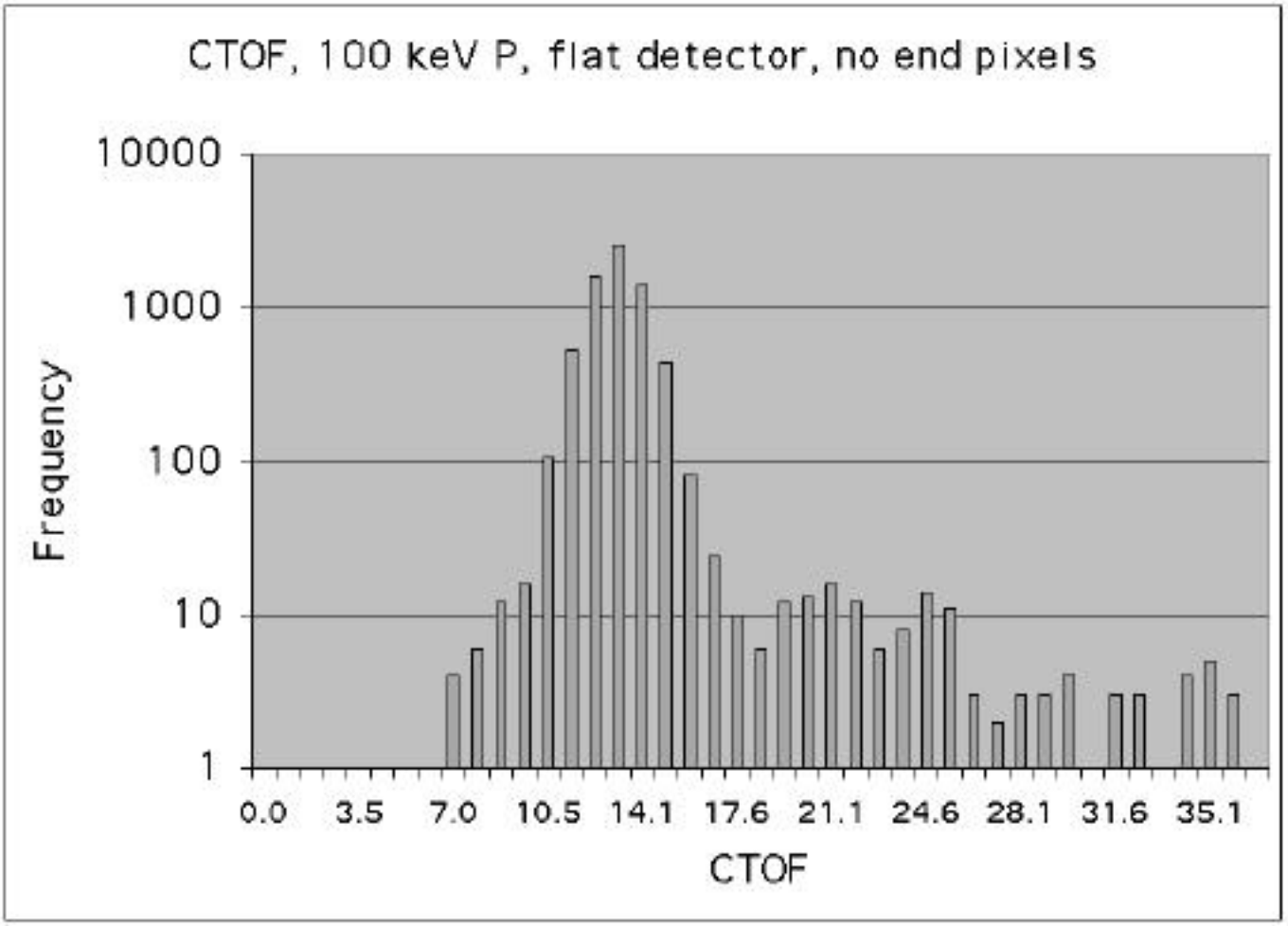

Figure 22 Histogram of CTOF, eliminating those pixels which are most prone to TOF double-peaking.

Xback \ Yback (cm)	4.53	4.11	3.69	3.27	2.85	1.89	1.47	1.05	0.63	0.21
0.21	82	88	86	85	87	231	229	230	232	226
0.63	94	92	90	89	91	235	233	234	236	238
1.04	93	95	73	78	74	218	222	217	239	237
1.46	72	68	79	77	76	220	221	223	212	216
1.88	*80*	84	81	83	14	158	227	225	228	*224*
2.29	6	7	11	9	10	154	153	155	151	150
2.71	5	4	3	2	1	145	146	147	148	149
3.13	19	23	21	27	*0*	*144*	171	165	167	163
3.54	22	*16*	18	17	8	152	161	162	*160*	166
3.96	129	131	12	13	*15*	159	157	156	110	106
4.38	132	*128*	120	116	127	101	102	103	107	105
4.79	121	126	122	124	125	100	99	98	97	*96*
5.21	143	141	142	140	138	118	115	119	117	123
5.63	134	133	135	139	137	*112*	114	113	104	111
6.04	136	130	60	61	63	207	205	204	108	109
6.46	70	*64*	66	65	56	200	209	210	*208*	214
6.88	67	71	69	75	*48*	*192*	219	213	215	211
7.29	53	52	51	50	49	193	194	195	196	197
7.71	54	55	59	57	58	202	201	203	199	198
8.13	*32*	36	33	35	62	206	179	177	180	*176*
8.54	24	20	*31*	29	28	172	173	175	164	168
8.96	45	*47*	25	30	26	170	174	169	191	189
9.38	46	44	42	41	43	187	185	186	188	190
9.79	34	40	38	37	39	183	181	182	184	178
(PHI)	39.5	36.8	33.9	30.7	27.4	19.0	15.0	10.8	6.5	2.2

These Pixels sometimes give low Energy

These Pixel IDs may be erroneous

These Pixels give spuriously high Energy

This Pixel is excessively noisy

Figure 23 Map of the positions of the SSD pixels, labeled by the pixel ID which is sent to the DPU with each SSD event. The color key identifies pixels that give spurious results of various degrees of importance.

The SSD calibration has turned up several quirks which must be tracked in producing images on-board. These include a set of pixels which very occasionally yield low measured energies; a smaller set which tend to give abnormally high energies; a third set for which the pixel ID is incorrect (a different, unknown pixel received an event, but one of this set of IDs was sent to the DPU), and an excessively noisy pixel.

The last category is, of course, a function of threshold settings. Such noisy pixels may be tuned to high energies and used there, only. All of these irregularities are tracked in flight software. In-flight calibration, both using radioactive sources on the inside of the shutter, and using an electronic calibrator in conjunction with selective powering of preamplifiers, will be used to periodically evaluate all of the pixels and adjust for aging, radiation, and temperature effects throughout the mission. Crosstalk between pixels is not a problem at the detector level, but is seen at the post-detection processing chip level. It is this cross-talk which accounts for the erroneous ID's that one group of pixels experience.

4. Data Reduction, Analysis, Archiving, And Distribution

Data reduction will take place initially at the spacecraft mission operations center. Reduction for analysis purposes will be conducted at APL.

4.1 DATA PRODUCTS

4.1.1 *Level-0 Data*

Each Level-0 data file will consist of a time-ordered set of source data packets from each instrument and a standard file header consistent with the ISTP Level-0 Guidelines (560-1DFD/0190). Two Level-0 data files will be generated for each instrument per orbit, a file of instrument science data packets, and a file of instrument housekeeping packets. The SMOC will post the most recent Level-0 data on the IMAGE web pages, in addition to providing it on a daily basis to the NSSDC. A quick-look version of each of these files will be generated immediately upon receipt of data from DSN, and a final version will be generated 3 days later, after recovering lost data.

4.1.2 *Level-1 Data*

In order to accomplish the IMAGE scientific goals, the ability to quickly survey a vast array of scientific data being generated by each instrument is essential. The result of Level-1 data processing in the SMOC is an image referred to as a Browse Product (BP). All BP data sets are created as Common Data Format (CDF) files using the ISTP Guidelines for Key Parameter Data. The SMOC will post the most recent BP data on the IMAGE web pages in addition to providing it on a daily basis to the NSSDC. A quick-look version of each of these files will also be generated immediately upon DSN pass completion. A delay of 3 days will occur if lost data needs to be recovered from DSN.

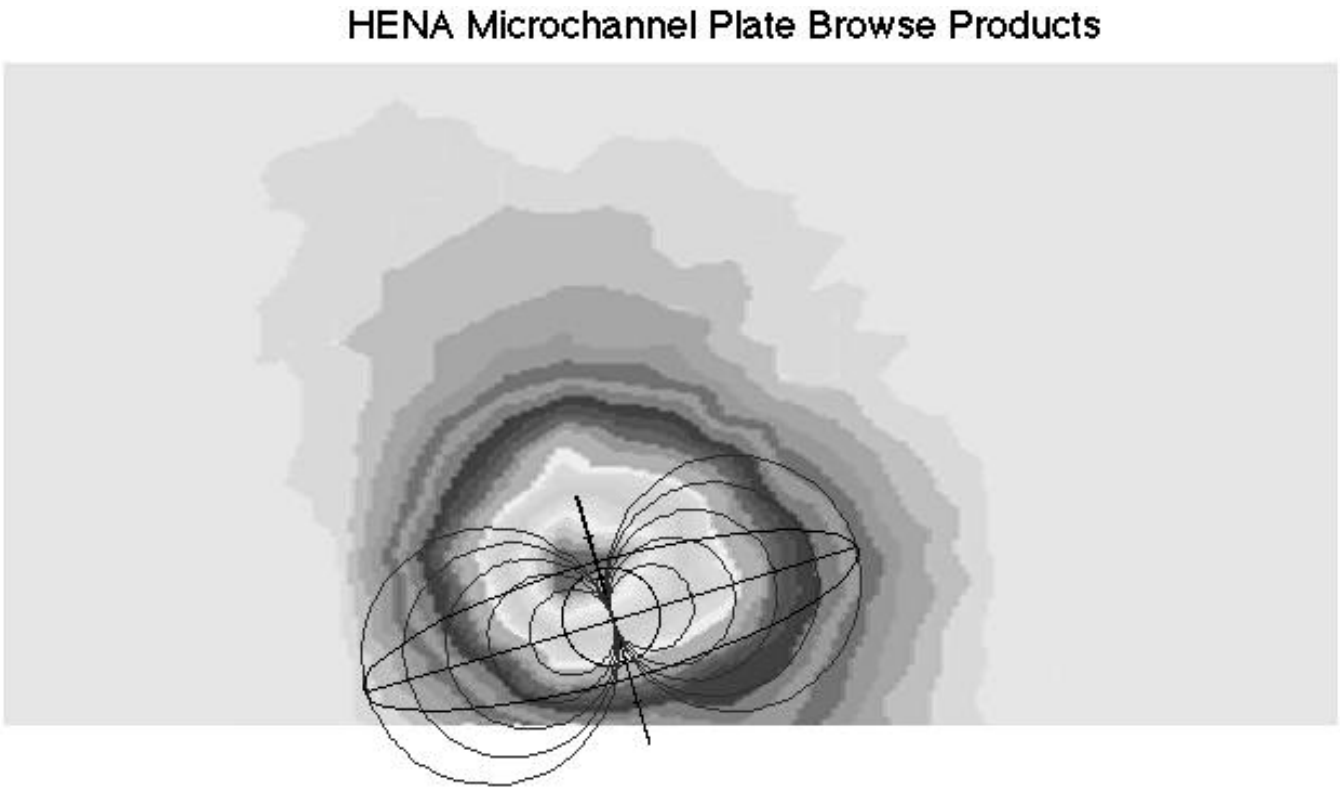

Figure 24 HENA Browse Product (schematic).

The software algorithms for the Browse Product production will be provided and integrated into the SMOC data production pipeline prior to the launch. The software and associated documentation for the Browse Products will be archived at the NSSDC.

4.1.3 *Level-2 and Higher Level Data Products*

Higher level IMAGE data products will be designed to illustrate magnetospheric structures and dynamics. All binary higher level data products will also be in the ISTP/Common Data Format. Each of the instrument teams (IT) have facilities at their institution that are used in processing, analyzing, and correlating IMAGE data. It is expected that some IMAGE investigators will routinely generate additional instrument data products. These products, along with associated documentation and the generation software, will be delivered to the NSSDC for long-term archiving and community-wide distribution.

The analysis required to generate the higher level products, and to derive scientifically meaningful quantities (ring current flux, spatial distribution, Dst, etc.), will depend heavily on both forward modeling and image inversion software currently being developed (Roelof and Skinner, 1999). As the software matures, it will be provided for general use, along with the archived data.

4.2 DATA ARCHIVING AND DISTRIBUTION

The Level-0, Level-1, attitude and orbit data products will be sent via FTP to the NSSDC daily for permanent archive and public distribution. These data products will only be held temporarily in the SMOC until they can be copied onto CD-ROM or DVD (Digital Versatile Disk) and sent to selected IMAGE investigators and participating scientists. The CD-ROMs/DVDs produced in the SMOC will conform to the ISO 9660 standard, which defines both the physical and logical format of the CD-ROM/DVD. This approach ensures that most CD-ROM/DVD drives on most platforms will be able to read these disks. In addition, the CD-ROM/DVD produced by the SMOC will follow other emerging NASA standards, guidelines, and practices, especially the use of Standard Formatted Data Unit (SFDU), and a file naming and directory structure which will be compatible with most platforms.

The National Space Science Data Center's (NSSDC's) on-line archive facility that will be used for rapid access to all the archived IMAGE data is called the NASA/NSSDC Data Archive and Distribution Service, or NDADS. The purpose of the NDADS system is to manage public archival data. Since the SMOC's primary purpose is to process and distribute the most recent IMAGE data, the SMOC is not designed to manage all the retrospective requests for older processed and archived IMAGE data. Investigators using IMAGE data who desire retrospective IMAGE data will be able to access the NSSDC's NDADS archive. NDADS provides archival data services not only to IMAGE scientists, but also to the worldwide science user community and the public.

One of the most important features of the NDADS system is that it provides the capability for scientists to retrieve data from the archive by several methods. The public data archive can easily be accessed through the NSSDC's automated retrieval mail system, or ARMS or the WWW. The NDADS system is operational 24 hours/day, 7 days/week and is a major archive and data distribution facility on the Space Physics Data System.

APPENDIX A

A. HENA Specifications

A.1 INTERFACES

A.1.1 *Mechanical*

*A.*1.1.1Mechanical Dimensions

The physical dimensions of the HENA MEU are shown in Figure A-1. The physical dimensions of the HENA sensor are shown in Figure A-2 .

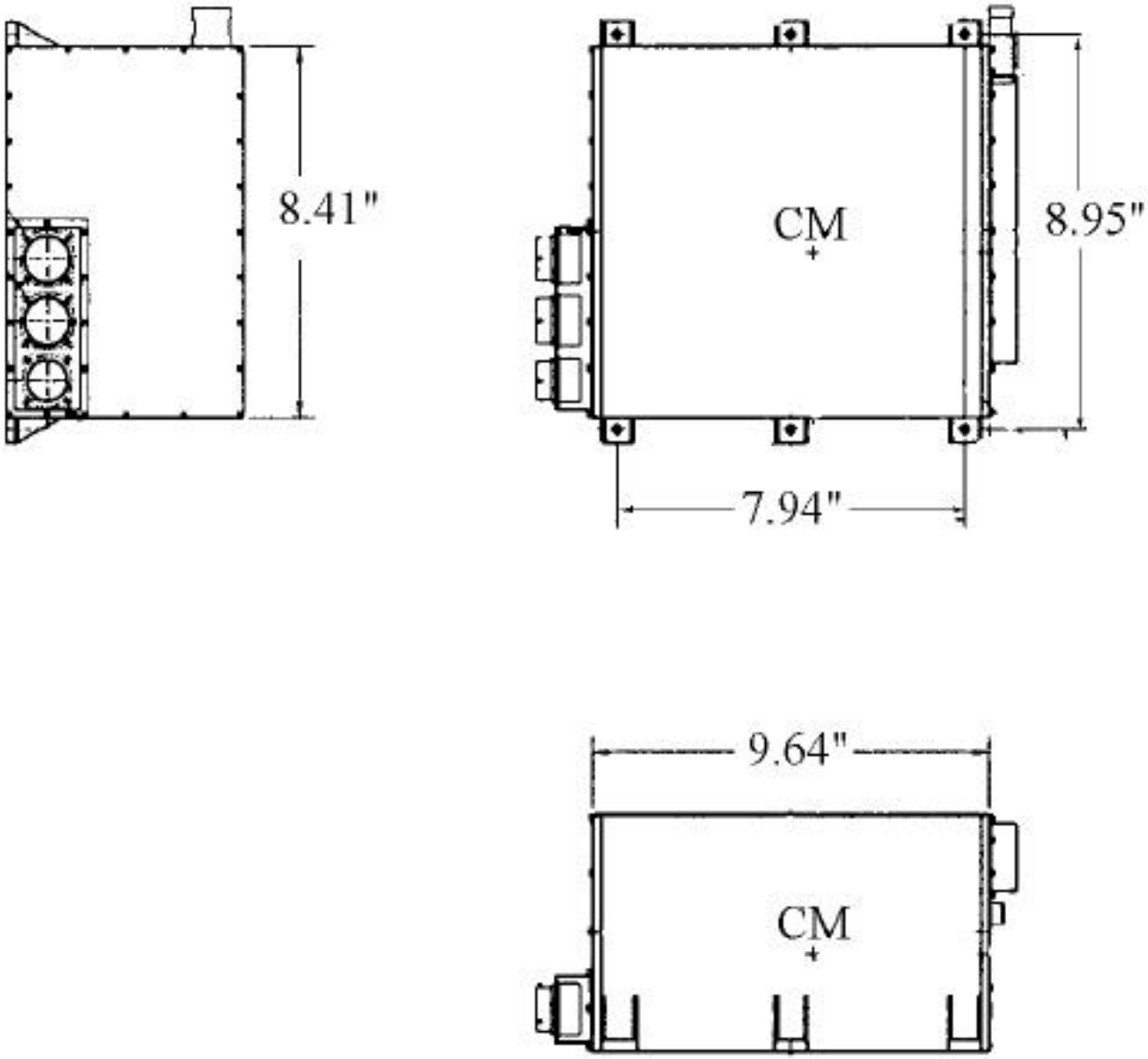

Figure A-1: HENA MEU dimensions

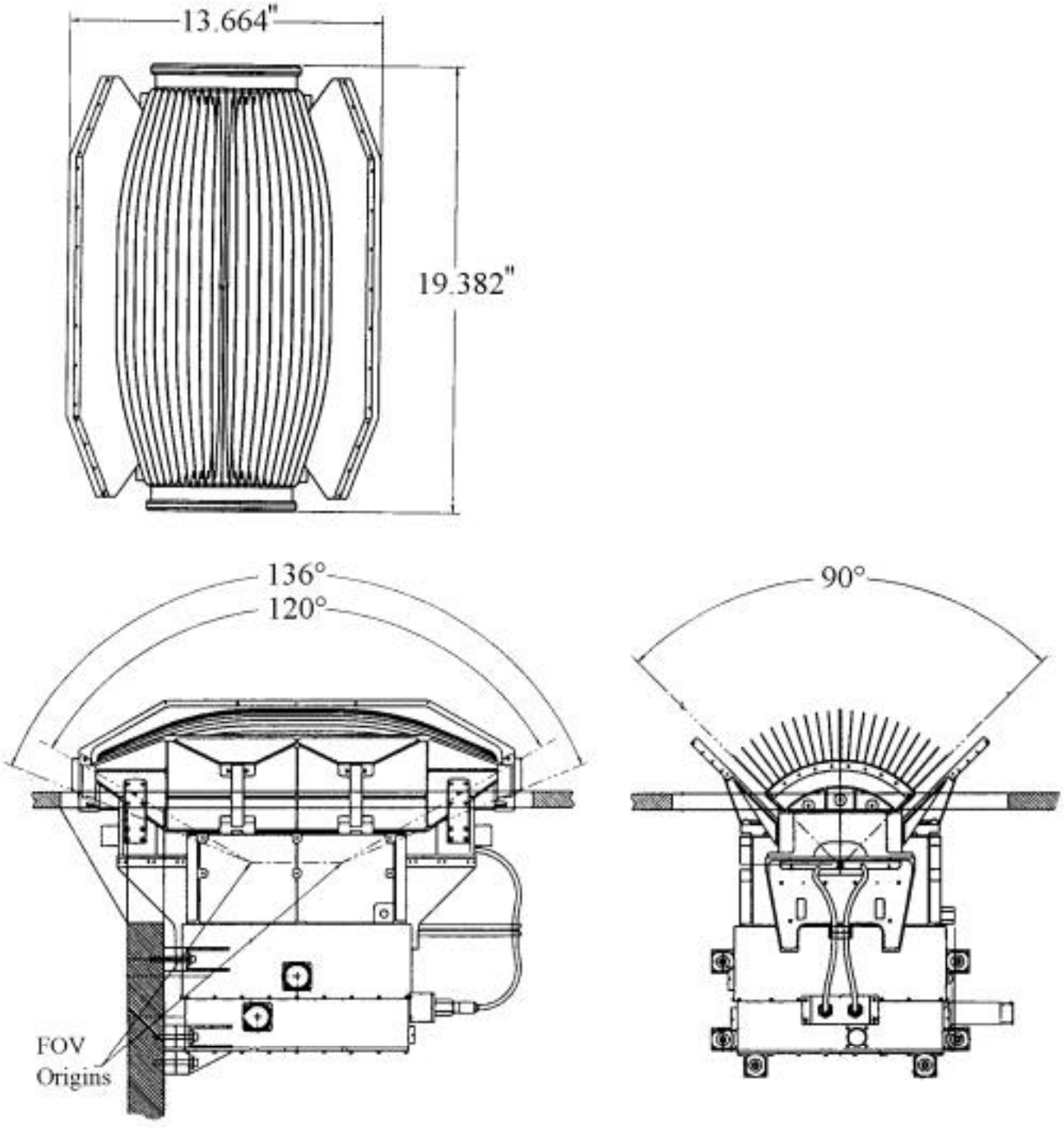

Figure A-2: Excerpt from HENA Sensor Interface Control Document.

A.1.1.2Mass Properties

The total mass of the HENA Imager is 19.05 kg. The mass properties associated with HENA are presented in the following table.

Table A-1: **HENA** Mass (less solar blankets, in kg)

Subsystem name	**Kg**
MEU	5.325
HENA Sensor & Bracket	12.87
Thermal Blanket	0.28
Cables	0.859
Instrument Total	19.05

A.1.1.3Radiation Design

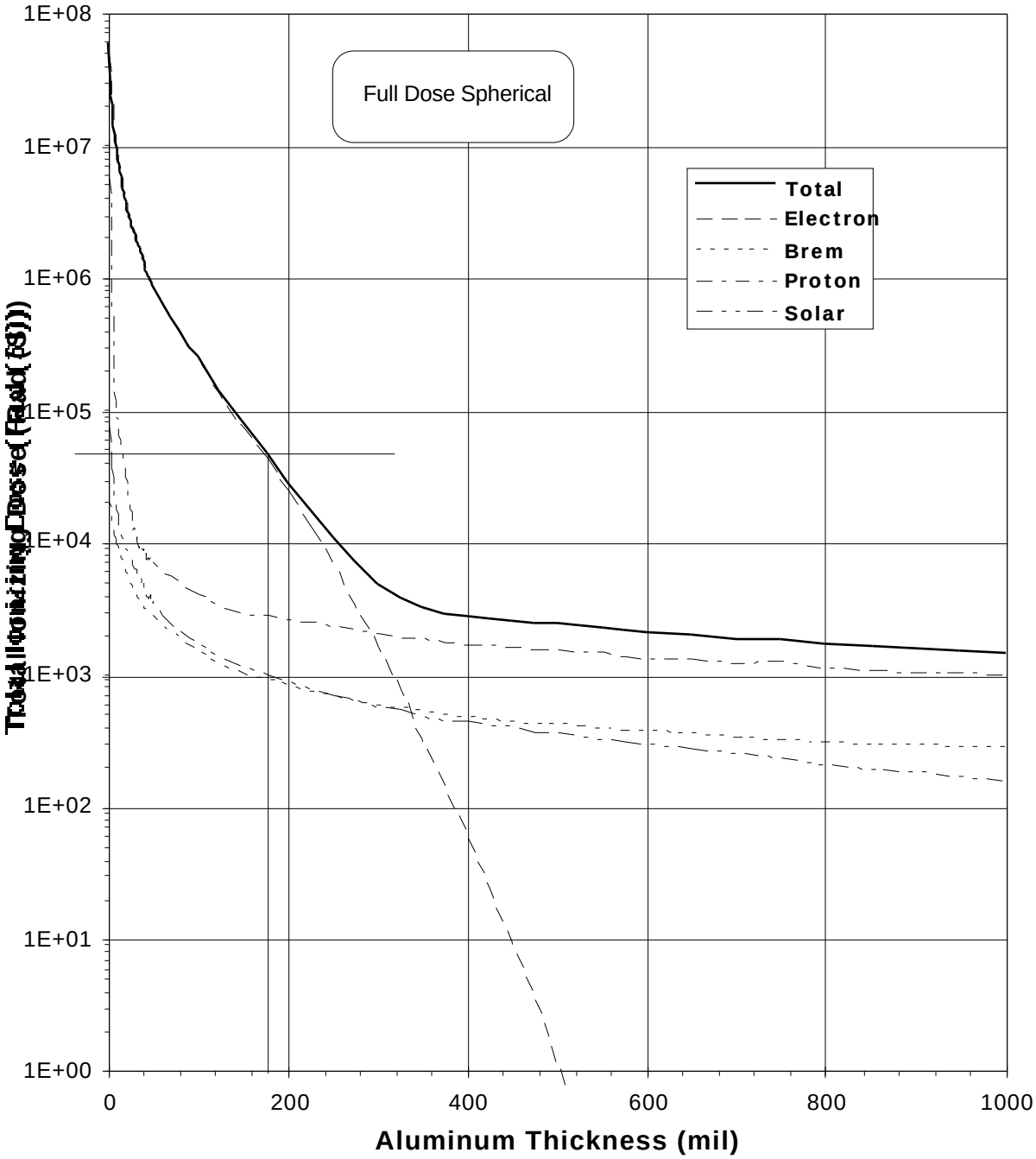

Figure A-3. Total ionizing dose for the 2-year IMAGE mission (Ref.: SwRI EM SYS-002) (guide lines added to indicate shielding level required for HENA design).

The Radiation Design Margin (RDM) is base-lined at a factor of 2, with 50 krads total dose selected as the target for HENA electronics. The radiation curve is based on a conservative spherical model and assumes no "shadowing." The HENA electronics are designed to a 100 krad dose tolerance, hence the factor of 2 margin. Based on the radiation curve in Figure A-3, HENA was built with 0.17" of aluminum shielding (or the equivalent). Of this, 0.018" of aluminum equivalent shielding is provided by the spacecraft walls and 0.070" of

aluminum equivalent shielding is provided by the payload deck. HENA box walls are 0.180" of aluminum. Spot shielding was used on selected parts as necessary, however with the heritage design from Cassini (100krad requirement), very little additional radiation design was necessary in HENA.

A.1.1.4 Deployables

A.1.1.4.1 Mechanical Properties of Instrument Deployables

A small (~15mm x 110 mm), hinged "door" protects the thin front foil from mechanical and acoustic damage. The door, located between the upper housing and the inside collimator plane, is released when a wax actuator pushes aside a restraining rod. This is a one-time operation (although the mechanism may be tested repeatedly on the ground).

- An electrical contact provides a telemetry indication that the door has opened; this is not active when the door is released.
- Opening the door provides a vent path for the purged sensor volume.
- The acoustic door latch and release mechanism is identical to Cassini/MIMI design.

The door release mechanism is also used to latch a fail-safe return spring (which holds the shutter open during launch) when the spring is cocked during a post-launch procedure. The shutter is rotated in front of the foil during flight by means of a stepper motor. Its normal ("open") position is away from the foil. The shutter may be moved repeatedly during flight as needed, and takes approximately 1 second to either open or close.

The shutter is used for the following purposes:

– Rotate a radioactive calibration source in front of the entrance slit
– Reduce the sensor geometry factor
– Provide some protection from solar EUV

A telemetry telltale is available to directly measure the shutter position, and will indicate when the door is either open or closed.

A.1.1.4.2 Method of acoustic door deployment

The HENA door is opened soon after launch. It will deploy via a wax actuator which performs open loop (actuator is self-safing). The deployment will be monitored via power delta (~10 watts) on 28V bus and door status indicator.

A.1.1.5 Field-of-View

The FOV is +/-60° perpendicular to the payload deck (polar angle, measured from the spin equator). The FOV is +/- 45° in azimuth (about HENA center of collimator; see Fig. A-2). This position provides for minimum viewing of RPI antennas, which deploy from adjacent facets of the spacecraft, 45° to either side of the center of the HENA FOV (see deck-plate layout, Fig. A-4).

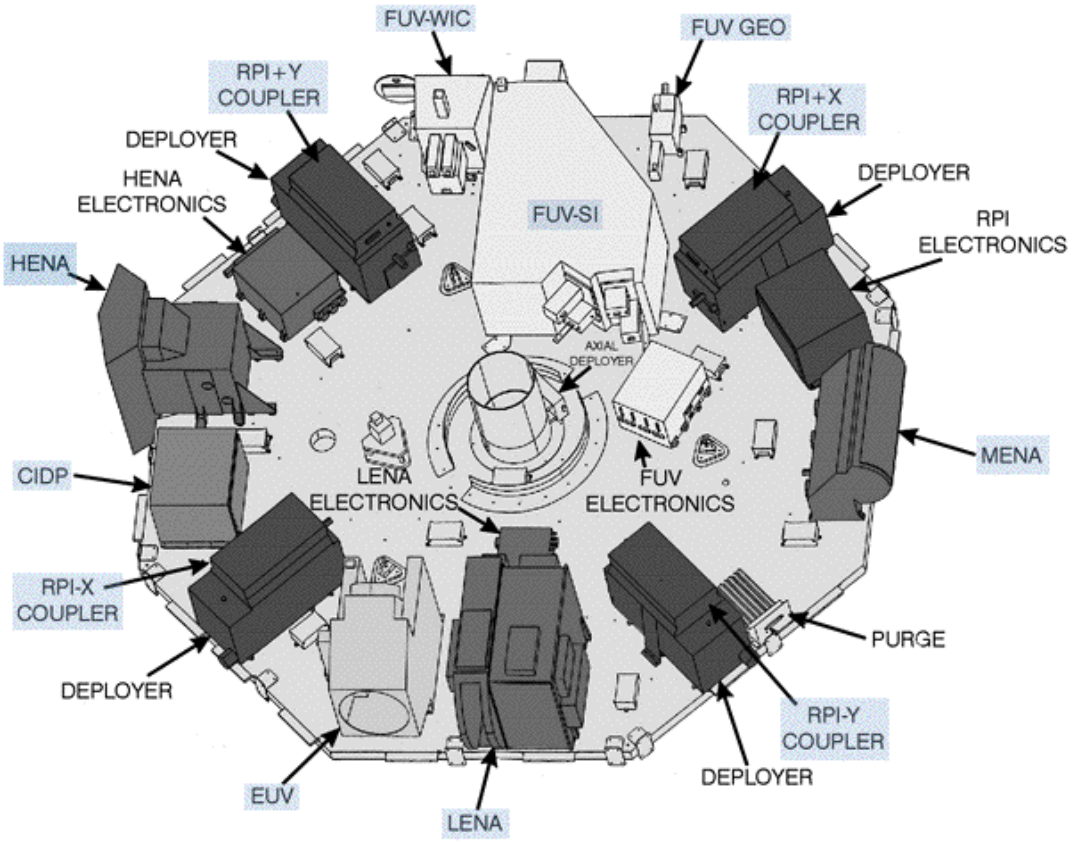

Figure A-4. HENA position on payload deck-plate

A.1.2 *Electrical*

A.1.2.1Power

The HENA instrument will use 14.6 W of orbit average power. Its peak power consumption will be <18.7 W. Power will be used according to the figures shown in Table A.1.2-1.

Table A.1.2 -1: HENA LVPS Output Requirements

Voltage	I (min) ma	I (nom) ma	I (max) ma	AC ripple	Regulation
+5V Analog	75	876	909	1%	5%
-5V Analog	67	236	238	1%	5%
+5V Digital	284	294	324	1%	5%
+15V	13	13	13	1%	5%
+30V	1	74	74	1%	5%

+70 (SSD Bias)	.005	.05	0.3	1%	5%

A.1.2.2 Power Profile and Peak Power

Table A.1.2-2: Average Power- CBE (watts primary power)

Mode	**Sensor**	**MEU**	**Total (CBE)**
Normal (Full Ops)	7.5	6.4	13.9
POR	3.0	3.5	6.5
Calibration (Full Ops+Cal)	7.2	6.5	13.7
Ambient Ops	4.9	5.4	10.3
Decontamination	15.0	0	15

*Note: Power distribution indicates location of thermal dissipation

Aside from inrush transients, power will remain quite close to nominal (normal), except for calibration periods, and use of decontamination heaters after launch.

In addition to the instrument modes discussed above, the decontamination mode is listed in this table. In this state, all instrument electronics are off. A 15W heater on the HENA sensor, supplied by the unswitched spacecraft heater interface, is powered on to prevent contaminants from coating the sensor surfaces during the first few weeks after launch. The decontamination heater is controlled by a latching relay inside the MEU. The MEU must briefly be powered on to command the relay to the ON state; the MEU will then be powered off to allow proper thermal dissipation on the payload deck.

A.1.3 *Command and Data Handling*

The CIDP provides a command interface to the HENA processor via the standard RS-422 serial interface. The format of the commands is as negotiated with the IMAGE Project. This means that the command information is a series of 16-bit command words that are simply passed from the CIDP to the HENA processor.

The HENA instrument is capable of executing some internally-timed command sequences, but in general, we will expect the CIDP to buffer and output appropriate command sequences from its own memory and command sequencer.

A.1.3.1Power On/Off Commands

These commands will switch power from the S/C to the instrument. The command is sent to the CIDP, which executes the action. These commands will be sent very infrequently.

A.1.3.2Memory Load Commands

These commands will be used to uplink patches to flight code and new parameter tables. HENA uses the standardized IMAGE Science Instrument memory load command format.

A.1.3.3Serial Digital Data

The CIDP provides a telemetry interface to the HENA processor via the standard RS-422 serial interface. HENA performs its own telemetry compression, so the instrument telemetry stream is simply put into CCSDS packets.

Data products are grouped in three categories: high resolution PHA event words, singles rates, and neutral particle image planes.

1) High resolution event words contain a complete record of the measured parameters for selected events. Only a limited number of these words can be sent through the telemetry stream, so an adaptive, rotating priority scheme is used to insure adequate coverage for rare events.

2) Singles rate channels are used to count events of a certain type, usually total counts from a given detector, or logic groups such as start-stop pairs, start, stop, and coincidence, start, stop, and energy, start and energy, etc. The rate data for single parameter measurements and logic elements are grouped separately in time for each 1/16 spin.

3) HENA neutral particle data are collected in 26 parallel image planes. Each plane will correspond to a different combination of spatial, time, energy, and mass resolutions. The microprocessor is responsible for selecting the appropriate image planes, generating the pixel address offset within the images, and incrementing the pixel counts. The image data are stored in the event memory in 16 bit deep pixels; the 26 image planes will require approximately 75 Kbytes of SRAM. Double buffering is used to collect the data in one buffer while reading it out of the other. This doubles the memory size required for the image event memory to 150 Kbytes of SRAM. It is our plan to use 256 Kbit SRAM for this purpose. To conserve telemetry the image data are log compressed to 8 bits/pixel, and further fast or Rice run-time encoded.

For HENA, there are essentially four different data types:

1) MCP back plane images; these are acquired as all-sky images, covering 360 degrees by 120 degrees, for 4 TOF (time of flight) ranges at ~3 degree pixel sizes. These will be produced once every spin, for an average rate of 1640 bps before image compression. Also among this type will be High TOF resolution images (6 TOF image planes), covering 360 x 120 degrees, at ~6 degree resolution, sent once per spin, for an average rate of 576 bps before image compression. Images produced are shown schematically in Fig. A-5.

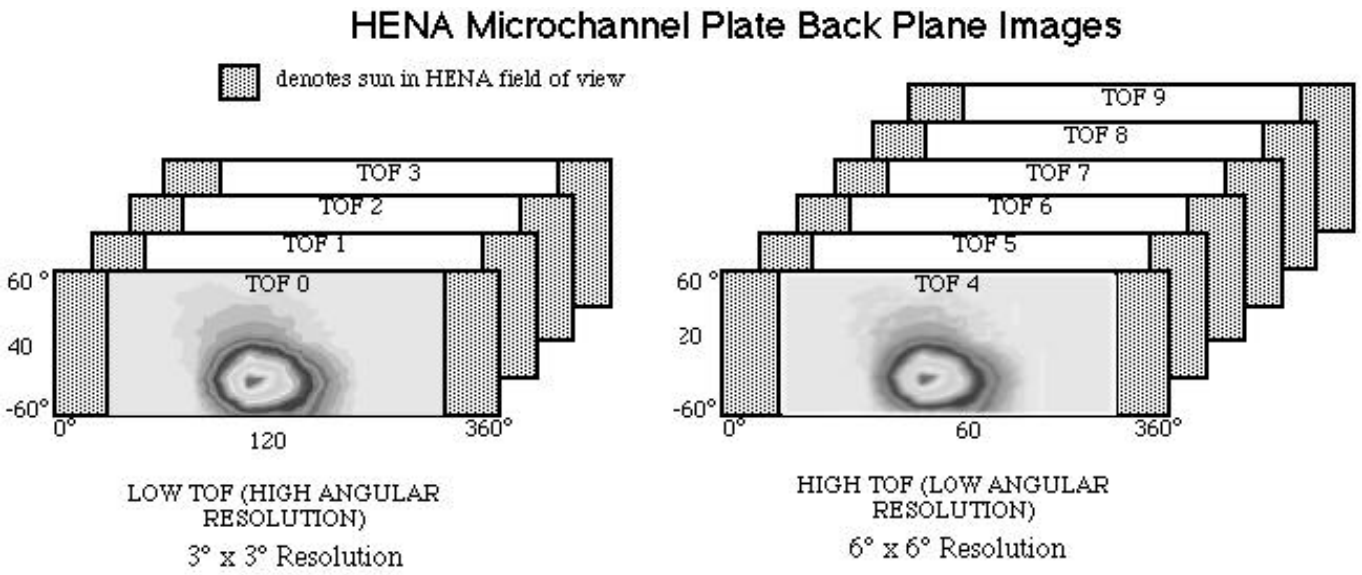

Figure A-5. HENA microchannel plate back plane images (schematic)

2) SSD back plane images; these are also acquired as all-sky images, also 360 X 120 degrees. These will be built up separately for Hydrogen, Helium, Oxygen, and Other, each for 4 different energy ranges, and will be sent once per spin at ~8 degree resolution, for an average rate of 1092 bps before image compression. The total bit-rate for these images, which assumes no compression and 16-bit deep pixels, is 2270 bps. Log compression from 16 to 8 bits reduces this to 1135 bps, which leaves room, for example, to increase the time resolution on the high resolution images to single spin resolution. Additional compression by a factor of ~2 may be achieved by Rice or "fast" run-time compression.

3) MCP back plane Pulse Height Analysis; events are transmitted at full useful resolution in pulse-height (front and back MCP), TOF, and position (angle). HENA will use its remaining data rate allocation between this data category and the next (with a small reserve for housekeeping).

4) SSD back plane Pulse Height Analysis; events are transmitted at full useful resolution in pulse-height (front MCP and back SSD), TOF, and position (angle).

These latter data categories will permit analysis of minor species, as well as higher resolution images at full mass, energy, and/or TOF resolution. All data are expected to packaged in self-contained sub-packets, with their own header information. HENA data are contained in downlink packets classified according to APIDs, as shown in Table A.1.3.3-1

Table A.1.3.3-1 HENA Telemetry APIDs

APID	Fixed Size?	Size (bytes)	Housekeeping?	Production	Description
0	Yes	28	No	periodic	Accumulators
1	No	1032	No	periodic	HENA-M PHA Results
2	No	1032	No	periodic	HENA-S PHA Results
3	No	1016	No	periodic	HENA-M Raw + PHA Results

4	No	1032	No	periodic	HENA-S Raw + PHA Results
5	No	610	No	periodic	High Resolution Image
6	No	310	No	periodic	Low Resolution Image
7	No	490	No	periodic	SSD Image
8	Yes	268	No	on demand	Memory Dump
9	Yes	14	No	on demand	Memory Checksum
10	Yes	200	No	on demand	Parameters
11	Yes	323	No	on demand	Calibration Sequences
12	Yes	82	No	on demand	Monitor Limits
13	Yes	1004	No	on demand	SSD Parameters
14	Yes	18	No	periodic	Schedule
15	Yes	520	No	on demand	Macro Status
64	Yes	110	Yes	periodic	Status
65	Yes	20	Yes	as needed	Command Echo
66	Yes	12	Yes	as needed	Alarm

A.1.3.4Health and Safety

The HENA DPU has some health and safety monitors built into its software. If an alarm condition is detected that the HENA software cannot handle, it will set an alarm flag in the telemetry sent to the CIDP. The CIDP turns off the instrument power upon receipt of this flag. There can be up to a two minute delay between when the alarm is declared and when the CIDP reads the flag, due to data buffering within the CIDP.

The HENA instrument is capable of executing some internally-timed command sequences, but in general, we expect the CIDP to buffer and output appropriate command sequences from its own memory and command sequencer with timing precision at the level of the 0.1 degree spin phase pulse (although for HENA, 1.0 degree accuracy would be adequate). Accurate spin position must be known onboard, to mitigate solar EUV flux.

The CIDP provides on-board knowledge of spacecraft and/or UT time to the HENA processor via the command interface. This information is used to time-tag the HENA telemetry packets, and to execute internal sequences (when necessary). This time will be accurate to better than 1 second, with resolution of 1 second or better. It will be sent to the HENA instrument at least once per spin, and will correspond to the time of the sun pulse on the 0.1 degree resolution spin pulse interface.

The DPU will monitor the spacecraft attitude with respect to the sun, and may temporarily lower the MCP HV levels during times that the sun will fall upon the front foil, if the shutter mechanism is not sufficient.

A.1.4 *Central Instrument Data Processor*

*A.*1.4.1Data Transfer Rate

The expected data transfer rate to the CIDP will be 38.4 kbps. During any 13.5 hour spacecraft orbit period, the total amount of data transferred will be limited to 135000 kbits at most.

A.1.5 *Thermal*

*A.*1.5.1Thermal Design Requirements

The HENA sensor will operate preferentially between 0 and +20°C. Although a lower temperature would normally be preferred to help keep the SSD noise down to minimum levels, the SSD system exhibits digital noise which feeds back into the AMPTEK 225 preamps at low temperatures. This feedback is minimized above about 0°. This temperature range is needed for operations only; the sensor may be operated during test over a much larger range. The sensor is thermally isolated from the payload and spacecraft structures with isolators at the mounting feet and thermal blankets between the sensor and the surrounding structure. Heat is radiated away to space via the sensor collimator.

The MEU is thermally and mechanically mounted directly to the payload deck.

In addition to the decontamination heaters, for the thermally isolated sensor head, there is an always-on (after third stage burn, at least) +28V and return power supply to the sensor head (via the MEU) for survival heat. This is separate from the rest of the HENA 28V supply. The heater that line supplies is turned on by a thermostat on the sensor head whose temperature is set to the survival temperature of the sensor. The thermostat maintains the sensor head at minimum survival temperature even when the rest of the HENA instrument is powered off. The 28V supply line, on its way through MEU, also feeds a solid state switch the output of which goes directly to the sensor head heater. (This forms an effective wired OR circuit where either the solid state switch or the thermostat can activate the heater.) Normal operating temperature and temperature at turn-on are maintained by the MEU using the solid state switch to supply power to the heater; when used in this manner, the survival heater is referred to as the "Replacement Heater".

*A.*1.5.5Thermal Finish

HENA collimator is finished with surfaces appropriate to maintain thermal balance within the preferred operating temperature range while isolated from the spacecraft deck, and without the use of supplemental heaters.

*A.*1.5.6Temperature Range

The HENA MEU and Sensor have the following flight allowable temperature ranges and stability.

MEU: -15 to +50°C non-op; -10 to + 45°C op; 0 to +30°C flight preferred; switch-on -15 to +50°C

Sensor:-25 to +40°C non-op; -20 to + 20°C op; -20 to + 35°C ground op; -20 to +5°C flight preferred; switch-on -25 to +40°C.

Thermistors in sensor head and MEU are monitored by the HENA DPU.

A.2 SPECIAL GROUND SUPPORT EQUIPMENT (GSE)

A.2.1 *Electrical GSE*

The instrument GSE is based on GSEOS software running on Pentium computers. The large majority of the GSE software are inherited from Cassini/MIMI, but the spacecraft interface software and hardware has been modified. In particular, an RS422 interface card is used. The spacecraft power bus emulation has a +28V power supply for spacecraft primary power bus. The S/C custom solid state current limiter is emulated.

Cassini MIMI Special Test Equipment Block Diagram

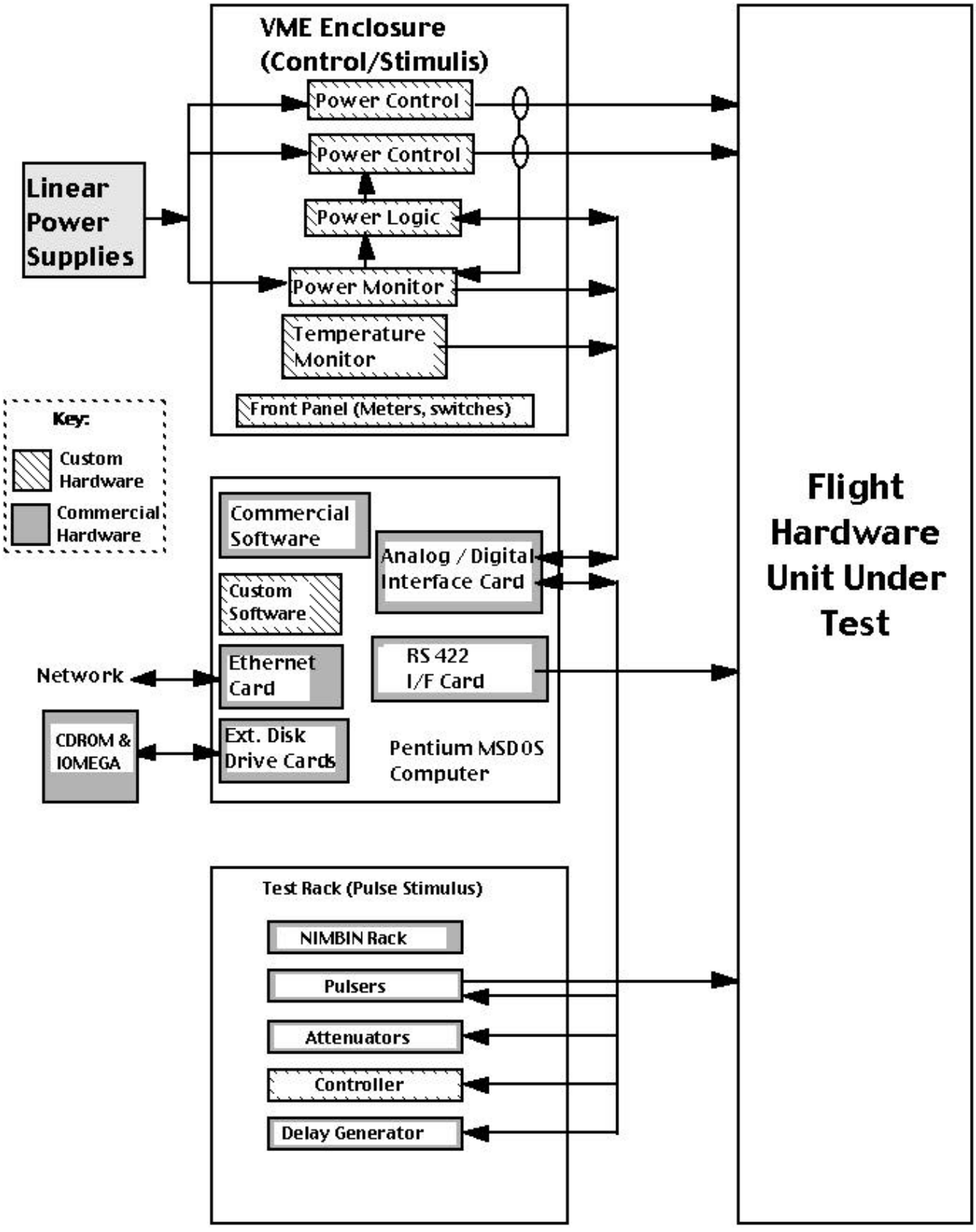

Figure A-6. GSE Block Diagram.

Acknowledgements

The authors gratefully acknowledge all of the many individuals who spent considerable time and care in building the HENA instrument, with special thanks to Bill Gibson and Jim Burch for their strong support; much thanks also to Herb Funsten and Dave McComas for help with the shutter and other technical support and information; to Stefano Livi for technical support, consultation, and help with evaluating the SSDs; to Chris Gurgiolo for invaluable help with downlink processing; to Martha Kusterer for ground software support; and finally to Ed Roelof, Barry Mauk, Don Williams, Andrew Skinner, Chris Chase, and Michael Hesse for scientific input, modeling efforts, and all the years of work that went into developing the techniques for ENA imaging.

References

Barabash, S., Norberg, O., Lundin, R., Olsen, S., Lundin, K., C:son Brandt, P., Roelof, E. C., Chase, C. J., Mauk, B. H., Koskinen, H., and Rynö, J.: 1998, "Energetic neutral atom imager on the Swedish microsatellite Astrid", *Measurement Techniques in Space Plasmas, Fields, R. F. Pfaff, J. E. Borovsky, and D. T. Young, ed., AGU Geophysical Monograph* **103**, 257.

C:son Brandt, P., S. Barabash, S., Norberg, O., Lundin, R., Roelof, E. C., and Chase, C. J.: 1999a, "Energetic neutral atom imaging at low altitudes from the Swedish microsatellite Astrid: Images and spectral analysis", *J. Geophys. Res.*, **104**, 2367

C:son Brandt, P., S. Barabash, S., Norberg, O., Lundin, R., Roelof, E. C., and Chase, C. J.: 1999b, "Energetic neutral atom imaging at low altitudes from the Swedish microsatellite Astrid: 2. Extraction of the ion distribution and implications for O^+ precipitation", in press, *J. Geophys. Res.*.

Funsten, H. O., McComas, D. J., Moore, K. R., Scime, E. E., and Thomsen, M. F.: 1994, "Imaging of magnetospheric dynamics using low energy neutral atom detection," *Solar System Plasmas in Space and Time, Geophysical Monograph* **84**, 275.

Funsten, H. O., McComas, D. J., and Gruntman, M. A.: 1998, "Neutral atom imaging: UV rejection techniques," *Measurement Techniques in Space Plasmas: Fields, eds.,R. F. Pfaff, J. E. Borovsky and D. T. Young, AGU Geophysical Monograph Series Vol.* **103**, 251.

Gruntman, M. A.,: 1997, "Energetic neutral atom imaging in space plasmas", *Rev. Sci. Instrum.* **68(10)**, 3617.

Henderson, M. G., Reeves, G. D., Spence, H. E., Sheldon, R. B., Jorgensen, A. M., Blake, J. B., and Fennell, J. F.: 1997, "First energetic neutral atom images from Polar", *Geophys. Res. Lett.*, **24**, 1167.

Hesse, M., and Birn, J.: 1998, "Neutral atom imaging of the plasma sheet: fluxes and instrument requirements", *Measurement Techniques in Space Plasmas: Fields, eds.,R. F. Pfaff, J. E. Borovsky and D. T. Young, AGU Geophysical Monograph Series Vol.* **103**, 297.

Hsieh, K. C. and Curtis, C. C.: 1998, "Imaging space plasma with energetic neutral atoms above 10 keV" *Measurement Techniques in Space Plasmas: Fields, eds.,R. F. Pfaff, J. E. Borovsky and D. T. Young, AGU Geophysical Monograph Series Vol.* **103**, 235.

Hsieh, K. C., Sandel, B. R., Drake, V. A., and King, R. S.: 1991, "H Lyman α transmittance of thin C and Si/C foils for keV particle detectors," *Nuc. Inst. Meth.*, **B61**, 187.

Hsieh, K. C., Keppler, E., and Schmidtke, G.: 1980, "Extreme ultraviolet induced forward photoemission from thin carbon foils," *J. Appl. Phys.*, **51**, 2242.

Keath, E. P., Andrews, G. B., Cheng, A. F., Krimigis, S. M., Mauk, B. H., Mitchell D. G., and Williams, D. J.: 1989, "Instrumentation for energetic neutral atom imaging of magnetospheres," *Solar*

System Plasma Physics, J. H. Waite, Jr., J. L. Burch, and R. L. Moore, Ed., AGU Geophysical Monograph **54,** 165.

Krimigis, S. M., Mitchell, D. G., Hamilton, D. C., Livi, S., Dandouras, J., Jaskulek, S. E., Armstrong, T. P., Cheng, A. F., Gloeckler, G., Hsieh, K. C., Ip, W. –H., Keath, E. P., Kirsch, E., Krupp, N., Lanzerotti, L. J., Mauk, B. H., McEntire, R. W., Roelof, E. C., Tossman, B. E., Wilken, B., and Williams, D. J.: 1999, "Magnetosphere imaging instrument (MIMI) on the Cassini mission to Saturn/Titan", *Space Sci. Rev., in press*.

Lui, A. T. Y., Williams, D. J., Roelof, E. C., McEntire, R. W., and Mitchell, D. G.: 1996, "First composition measurements of energetic neutral atoms", *Geophys. Res. Lett.*, **23**, 2641.

McComas, D.J., Funsten, H.O., Gosling, J.T., Moore, K.R., and Thomsen, M.F.: 1992, "Low energy neutral atom imaging", *Instrumentation for Magnetospheric Imagery, SPIE Proc., V.* **1744**, 40.

McComas, D.J., Funsten, H.O., Gosling, J.T., Moore, K.R., Scime, E.E., and Thomsen, M.F.: 1994, "Fundamentals of low energy neutral atom imaging," *Optical Engineering,* **33**, 335.

McComas, D.J., Funsten, H.O., and Scime, E.E.,: 1998, "Advances in low energy neutral atom imaging," *Measurement Techniques in Space Plasmas: Fields, eds. R. F. Pfaff, J. E. Borovsky and D. T. Young, AGU Geophysical Monograph Series Vol.* AGU **103**, 275.

McEntire, R. W., and Mitchell, D. G.: 1989, "Instrumentation for global magnetospheric imaging via energetic neutral atoms," *Solar System Plasma Physics, J. H. Waite, Jr., J. L. Burch, and R. L. Moore, Ed., AGU Geophysical Monograph* **54**, 69.

McEntire, R. W., Keath, E. P., Fort, D. E., Lui, A. T. Y., and Krimigis, S. M.: 1985, "The medium energy particle analyzer (MEPA) on the AMPTE CCE spacecraft," *IEEE Trans. Geosci. Remote Sensing,* **GE-23**, 230.

Meckbach, W., Braunstein, G., and Arista, N.: 1975, "Secondary-electron emission in the backward and forward directions from thin carbon foils traversed by 25-250 keV proton beams", *J. Phys. B*, **8**, L344.

Mitchell, D. G., Cheng, A. F., Drake, V. A., Hsieh, K. C., Krimigis, S. M., Keath, E. P., Jaskulek, S. E., Mauk, B. H., McEntire, R. W., Roelof, E. C., and Williams, D. J.: 1993, "INCA, the ion neutral camera for energetic neutral atom imaging of the Saturnian magnetosphere", *Optical Engineering,* **32** 3096.

Mitchell, D. G., Cheng, A. F., Hsieh, K. C., Krimigis, S. M., Keath, E. P., Jaskulek, S. E., Mauk, B. H., McEntire, R. W., Roelof, E. C., Schlemm, C. E., Tossman, B. E., and Williams, D. J.: 1998, "The ion neutral camera for the Cassini Mission to Saturn and Titan", *Measurement Techniques in Space Plasmas: Fields, eds. R. F. Pfaff, J. E. Borovsky and D. T. Young, AGU Geophysical Monograph Series Vol.* AGU **103**, 281.

Paschalidis, N. P.: 1998, "Microelectronics Technologies Enabling New Generation Spacecraft and Instrumentation", *in Science Closure and Enabling Technologies for Constellation Class Missions. Volume edited by The American Geophysical Union, UC Berkeley, California, December 1998* 123.

Paschalidis, N. P., Karadamoglou, K., Stamatopoulos, N., Paschalidis, V., Kottaras, G., Sarris, E., Keath, E., and McEntire, R.: 1998, "An Integrated Time to Digital Converter for Space Instrumentation", *proceedings of the 7th NASA Symposium on VLSI Design October 1998, Albuquerque, University Of New Mexico*, 541.

Powell, F. R.,: 1992, "Care and feeding of soft x-ray and extreme ultraviolet filters," *Laser-Induced Damage in Optical Materials: SPIE Proc.*, **1848**, 503

Powell, F. R., Vedder, P. W., Linblom, J. F., and Powell, S. F.: 1990, "Thin film performance for extreme ultraviolet and x-ray applications," *Opt. Eng.* **29**, 614.

Rairden, R. L., Frank, L. A., and Craven, J. D.: 1986, "Geocoronal Imaging with Dynamic Explorer," *J. Geophys. Res.*, **91,** 13,613.

Roelof, E. C.,: 1987, "Energetic neutral atom image of a storm-time ring current," *Geophys. Res. Lett.*, **14**, 652.

Roelof, E. C., Mitchell, D. G., and Williams, D. J.: 1985, "Energetic neutral atoms (E~50 keV) from the ring current: IMP 7/8 and ISEE-1," *J. Geophys. Res.*, **90**, 10991.

Roelof, E. C., and A. J. Skinner,: 1999, "Extraction of ion distributions from magnetospheric ENA and EUV images", *in review, Planetary and Space Sci.*

Williams, D. J., Roelof, E. C., and Mitchell, D. G.: 1992, "Global magnetospheric imaging", *Rev. Geophys.*, **30**, 183.
Williams, D.J., Keppler, E., Fritz, T.A., Wilken, B., and Wibberenz, G.,: 1978, "The ISEE 1 and 2 medium energy particles experiment", *IEEE Trans. Geosci. Electron.*, **GE-16(3)**, 270.